Novel expression of major histocompatibility complex II in dorsal root ganglion neurons attenuates paclitaxel-induced cold hypersensitivity in male and female mice

Authors: Emily E. Whitaker[1], Neal E. Mecum[1], Riley C. Cott[1] and Diana J. Goode[1]*

Affiliations: [1]Department of Biomedical Sciences, College of Osteopathic Medicine, University of New England, Biddeford, Maine 04005, USA

*Corresponding author. Email: dgoode@une.edu

Abstract

Chemotherapy is often a life-saving cancer treatment, but the development of intractable pain caused by chemotherapy-induced peripheral neuropathy (CIPN) is a major dose-limiting toxicity that restricts cancer survival rates. Recent reports demonstrate that paclitaxel (PTX) robustly increases anti-inflammatory $CD4^+$ T cells in the dorsal root ganglion (DRG), and that T cells and anti-inflammatory cytokines are protective against CIPN. However, the mechanism by which $CD4^+$ T cells are activated and the extent cytokines released by $CD4^+$ T cells target DRG neurons are unknown. Here, we demonstrate that $CD4^+$ T cells can directly contact DRG neurons, and we detected novel expression of functional major histocompatibility complex II (MHCII) protein in DRG neurons, together suggesting direct cell-cell communication and targeted cytokine release. MHCII protein is primarily expressed in small nociceptive neurons in male mouse DRG regardless of PTX treatment, while MHCII protein is induced in small nociceptive neurons in female mice after PTX. Accordingly, eliminating MHCII from small nociceptive neurons significantly increased hypersensitivity to cold temperature in only naïve male mice, while knocking out MHCII in small nociceptive neurons significantly increased the severity of PTX-induced

cold hypersensitivity in both female and male mice. Novel expression of MHCII in DRG neurons identifies a targeted mechanism to suppress not only CIPN but also possibly autoimmunity and neurological diseases.

Graphical abstract

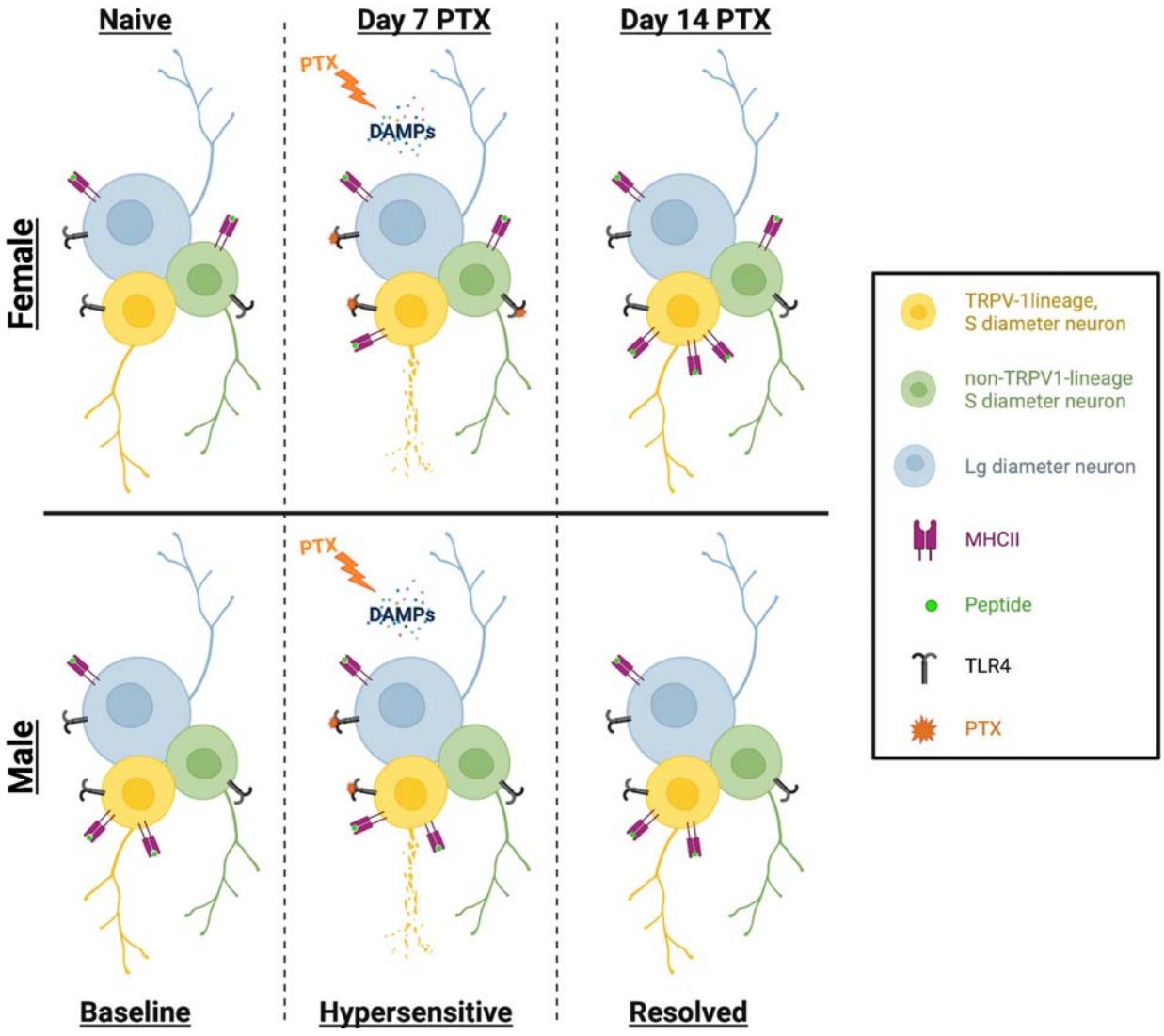

Created with Biorender.com

One Sentence Summary

Functional MHCII protein expressed on the surface of small diameter nociceptive neurons alleviates PTX-induced cold hypersensitivity in male and female mice.

INTRODUCTION

Paclitaxel (PTX) is an anti-neoplastic drug commonly used to treat breast, lung, and ovarian cancer(*1*). However, this life-saving cancer treatment is often dose-limiting as more than 60% of patients develop painful chemotherapy-induced peripheral neuropathy (CIPN)(*2*). Endothelial cells encapsulating dorsal root ganglia (DRG) have large fenestrations(*3*) with an altered repertoire of tight junction proteins(*4*) allowing PTX to enter the DRG and to bind to toll-like receptor 4 (TLR4) expressed on DRG neurons(*5*). Accumulation of PTX in the DRG results in neuronal hyperexcitability(*6-8*) and neurotoxicity(*9, 10*) manifesting as pain, tingling, and numbness in a stocking and glove distribution(*11*). Recently, T cells and anti-inflammatory cytokines have been shown to suppress CIPN; however, the underlying mechanism contributing to the resolution of CIPN remains elusive, which is evidenced by limited treatment options.

Both innate and adaptive immune cells are present at a low abundance in the DRG of naïve male(*12*) and female(*13*) mice. Consistent with the blood(*14*), naïve female mice have more $CD4^+$ T cells in the DRG compared to male mice(*13*). While treatment with PTX increases anti-inflammatory $CD4^+$ T cells more robustly in female mouse DRG(*13*), the mechanism by which this occurs is unclear.

It is thought that communication between $CD4^+$ T cells and neurons primarily occurs through the release of soluble mediators as neurons express cytokine receptors(*15*) while $CD4^+$ T cells express receptors for neurotransmitters(*16*). Pro-inflammatory $CD4^+$ T cell subsets (Th1 and Th17) secrete cytokines that sensitize neurons in the DRG and spinal cord to increase nociceptive-signaling(*17, 18*) while anti-inflammatory subsets (FoxP3 Tregs and Th2) secrete IL-10 and IL-4 to suppress activity in sensitized nociceptors and reduce neuronal hyperexcitability(*19*), respectively. Although $CD4^+$ T cell–neuron communication through soluble mediators has been more extensively studied, published DRG neuron RNA seq datasets (mouse and human(*20, 21*)) indicate direct cell-cell interaction is possible. By mining these single cell RNA seq data sets, we found that DRG neurons express major histocompatibility

complex II (MHCII) transcripts(*22, 23*), but there are no reports that show MHCII protein or function in DRG neurons.

MHCII is traditionally thought to be constitutively expressed on antigen-presenting cells (APCs) and induced by inflammation on some non-APCs, including endothelial, epithelial, and glial cells(*24*). In contrast to these non-APCs, human neural stem cells (hNSCs) and neural progenitor cells within embryo spinal cord and DRG constitutively express MHCII protein prior to the development of the adaptive immune response(*25*). Differentiating hNSCs to neurons in vitro increased MHCII, and inflammatory stimuli (IFN-γ) further elevate its expression(*25*), suggesting the possibility of MHCII on neurons in vivo. MHCII expression on neurons would provide insight into the mechanism by which $CD4^+$ T cells contribute to pain and neurological diseases.

While DRG neurons are wrapped with satellite glial cells (SGCs), sciatic nerve injury and nerve transection models demonstrate that immune cells can breach the SGC and lie directly against the neuron(*26*), suggesting direct neuron-immune communication can occur. Here, we found that $CD4^+$ T cells can contact DRG neurons directly in both naïve and PTX-treated mice, indicating $CD4^+$ T cells and DRG neurons can interact during homeostatic and inflammatory conditions.

Based on these findings, we sought to determine if DRG neurons express MHCII under homeostasis, and the extent PTX-induced inflammation modulates MHCII expression. Furthermore, we investigated the degree that neuronal MHCII contributes to the resolution of PTX-induced peripheral neuropathy. Our results confirm that DRG neurons do indeed express functional surface-bound MHCII protein, and that neuronal MHCII represents a novel mechanism to suppress CIPN, which could be exploited for therapeutic intervention against not only pain but autoimmunity and neurological diseases.

RESULTS

CD4$^+$ T cells can directly contact neurons in mouse DRG

We recently demonstrated that CD4$^+$ T cells in the DRG primarily secrete anti-inflammatory cytokines(*13*). IL-4 and IL-10 in particular have been shown to directly act on DRG neurons in vitro to suppress hyperexcitability and ongoing activity in sensitized nociceptors(*19, 27, 28*). However, the extent cytokines released by CD4$^+$ T cells target DRG neurons in vivo is unknown. Due to their short half-life, cytokine release typically occurs in close proximity to the target cell, but in the DRG, neurons are wrapped with SGCs, possibly impeding neuron access to cytokines. However, natural gaps in the glial envelope can occur(*29*), which may allow ingress by CD4$^+$ T cells. Therefore, initial fluorescent imaging experiments were designed to visualize CD4$^+$ T cells in close proximity to neurons in DRG tissue. To increase the likelihood of detecting CD4$^+$ T cell–DRG neuron contact sites, we utilized female mice as we have previously shown that the frequency of CD4$^+$ T cells in female mouse DRG is higher than male(*13*). We found that CD4$^+$ T cells frequently clustered in DRG tissue in close proximity to neurons **(Fig. 1A)**. Confocal microscopy was required to demonstrate that CD4$^+$ T cells colocalized with neurons in the absence of SGC markers (GLAST/FABP7) in DRG tissue from naïve and day 14 PTX-treated female mice **(Fig. 1B, C, Fig. 1S)**. Z-stacks of DRG tissue confirmed that CD4$^+$ T cells were located between the border (identified by differential interference contrast microscopy) of DRG neurons and SGCs (**Fig. 1B**, **Fig. S1**). Furthermore, we frequently observed that CD4$^+$ T cells appeared flattened at the contact interface (**Fig. 1B**, **C**, **Fig. S1**), suggesting DRG neurons may activate CD4$^+$ T cells. Our results demonstrate that CD4$^+$ T cells can breach SGCs and be in direct contact with DRG neurons, suggesting CD4$^+$ T cell–DRG neuron communication can occur through both cell-cell contact and the release of soluble mediators.

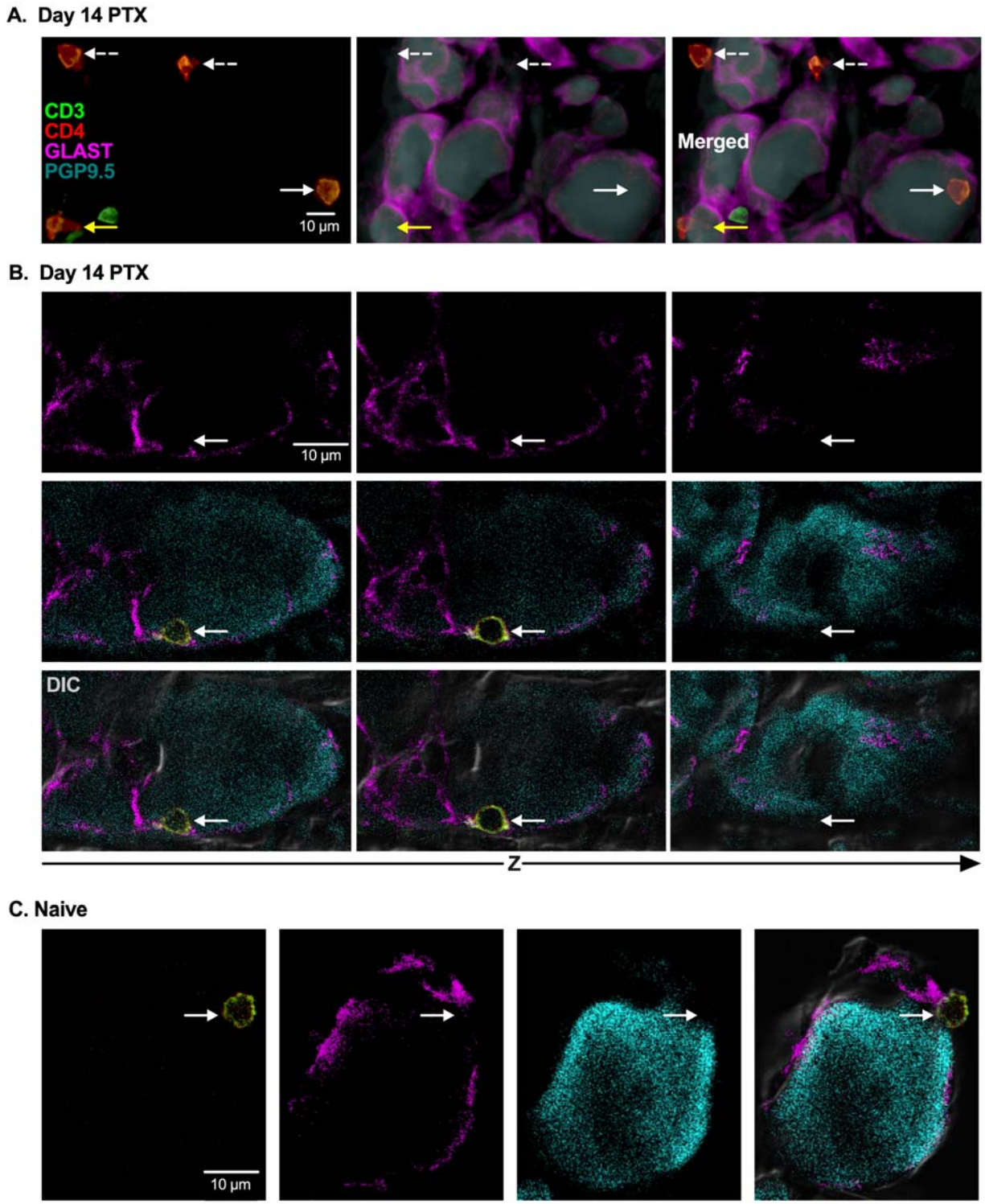

Fig. 1. CD4$^+$ T cells directly contact neurons in DRG tissue from naïve and PTX-treated female mice. (A-C) Immunohistochemical staining of neurons (PGP9.5: cyan), SGCs (GLAST: magenta), and T cells (CD3: green, CD4: red) in L4 DRG tissue from naïve and PTX-treated female mice. White arrows =

location of $CD4^+$ T cell. **(A)** Representative widefield epifluorescence two-channel (CD3/CD4; GLAST/PGP9.5) and merged images of $CD4^+$ T cells and DRG neurons in close proximity (solid arrow = absence of GLAST; dashed arrow = occluded by GLAST; yellow arrow = $CD4^+$ T cell extensions near a DRG neuron; n=5). **(B)** Differential inference contrast (DIC), fluorescence, and merged confocal Z-slice images of a $CD4^+$ T cell in direct contact with a $PGP9.5^+$ DRG neuron from a PTX-treated mouse. **(C)** Maximum projection images of a $CD4^+$ T cell in contact with a DRG neuron from a naïve mouse.

To identify immune molecules that might facilitate communication between $CD4^+$ T cells and DRG neurons upon cell-cell contact, we screened human and mouse(*22, 30*) DRG neuron RNA seq data sets. Our screen identified MHCII and MHCII-associated genes **(Fig. S2)**, which are critical for the activation of $CD4^+$ T cells. The presence of MHCII and MHCII-associated RNA transcripts in DRG neurons supports the possibility of direct $CD4^+$ T cell activation and targeted cytokine release. Consistent with the RNA seq data, we found RFX1 protein, a transcription factor for MHCII, in the nucleus of DRG neurons in male and female mice **(Fig. S3)**, further supporting the possibility of MHCII protein in DRG neurons.

MHCII protein detected in DRG neurons

As inflammatory stimuli are known to increase the expression of MHCII in immune cells(*31*), female mice were injected with PTX to induce inflammation in the DRG to maximize the possibility of detecting neuronal MHCII protein. DRG neuron lysates from naïve and day 14 PTX-treated female mice were analyzed by western blot using an antibody against MHCII. Consistent with inflammatory stimuli boosting the expression of MHCII, DRG neurons from PTX-treated female mice had almost 2-fold more MHCII protein than DRG neurons from naïve female mice (29.78 ± 2.76 arbitrary fluorescent units (AFUs) from naïve to 52.23 AFUs ± 8.21 14 days post-PTX, normalized to tubulin, $p=0.0410$, n=4/condition) **(Fig. 2A, B)**.

Although the cell lysates used for western blot primarily consisted of DRG neurons, negative selection by magnetic-activated cell sorting (MACS) does not yield a cell sample that is 100% pure. Therefore, it is possible that the MHCII protein signal detected by western blot represents MHCII from contaminating non-neuronal cells. To verify that DRG neurons express MHCII protein, we visualized MHCII in cultured DRG neurons by immunocytochemistry (ICC). Nuclei were labeled with DAPI to eliminate the possibility that MHCII staining was the result of a contaminating non-neuronal $MHCII^+$ cell. Maximum projection images acquired by confocal microscopy demonstrate MHCII staining in DRG neurons from day 14 PTX-treated female mice compared to the isotype control (**Fig. 2C**). Z-stack images showed MHCII staining through the entire DRG neuron, suggesting both surface and intracellular MHCII **(Fig. 2D)**. Cellular and molecular assays together confirm the expression of MHCII protein in DRG neurons.

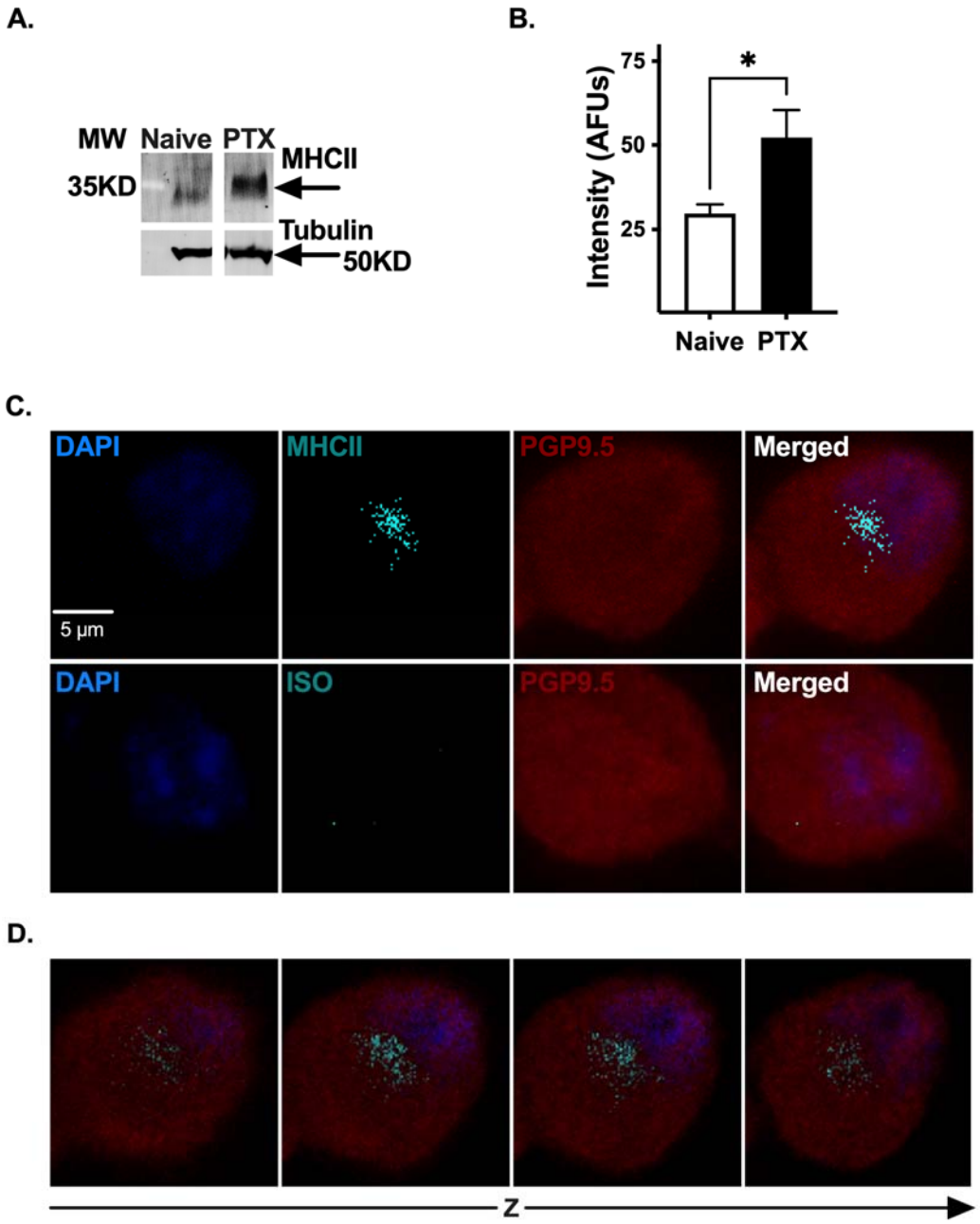

Fig. 2. DRG neurons from female mice express MHCII protein. (A) Western blot of MACS-DRG neuron lysates from naïve and day 14 PTX-treated female mice, probed with an antibody against MHCII and beta tubulin (loading control). **(B)** Quantification of MHCII band intensity normalized to tubulin for DRG neuron lysates from naïve (white bar) and day 14 PTX-treated (black bar) mice shown in **(A)**. Statistical significance determined by unpaired t-test (*p <0.05, n=4/condition). **(C, D)** Confocal images

of cultured DRG neurons from day 14 PTX-treated female mice with DAPI (blue), MHCII or isotype antibody (ISO: cyan), and PGP9.5 (red). **(C)** Representative single channel and merged maximum projection images of MHCII or ISO staining in DRG neurons, n=3. **(D)** Stepwise Z-slices of MHCII$^+$ neuron from **(C)**.

DRG neurons express surface-MHCII

MHCII expressed on the cell surface is required to activate CD4$^+$ T cells. Our confocal data suggests that DRG neurons express both intracellular and surface-MHCII. To confirm that neurons express surface-MHCII, we analyzed DRG neurons by flow cytometry. PGP9.5$^+$ neurons comprised 28.93% ± 2.33 of total DRG cells **(Fig. S4)**, and within the PGP9.5$^+$ neuron gate, 10.84% ± 1.73 of cells from naïve female mice expressed surface-MHCII **(Fig. 3A, B)**. The expression of MHCII on the surface of DRG neurons increased 2-fold after treatment with PTX (19.57% ± 1.17, p=0.0157, n=3) **(Fig. 3A, B**), which is consistent with inflammation increasing the half-life of surface-MHCII on APCs(*32*). MHCII on the neuron surface suggests a mechanism by which CD4$^+$ T cells could directly communicate with DRG neurons.

CD4$^+$ T cells respond to specific peptide bound to surface-MHCII; however, it is unknown if surface-MHCII on neurons can present peptide. To address this question, we cultured DRG neurons from naïve and day 14 PTX-treated female mice with FITC-conjugated OVA peptide. We found that PGP9.5$^+$ DRG neurons from naïve mice expressed surface-MHCII **(Fig. 3C)**, which co-localized with the OVA-FITC signal **(Fig. 3C)**, suggesting OVA peptide is bound to surface-MHCII. Of note, some naïve DRG neurons have diffuse OVA-MHCII signal (**Fig. 3C, solid white arrow**) while others have punctate (polarized) OVA-MHCII staining (**Fig. 3C, dashed white arrow**). PTX treatment in vivo significantly increased surface-MHCII on cultured neurons compared to neurons from naïve female mice (**Fig. 3D,** 64.87 ± 2.29

AFUs naïve to 87.59 ± 4.07 AFUs day 14, p=0.0083, n=3). Likewise, the intensity of OVA increased >2-fold on neurons from day 14 PTX-treated female mice compared to neurons from naïve female mice (**Fig. 3E,** 41.30 ± 3.10 AFUs naïve to 85.62 ± 4.80 AFUs day 14, p=0.0015, n=3). In addition, the area of polarized MHCII per neuron increased >4-fold after PTX (5.5% ± 1.26 naïve to 23.67% ± 1.12 day 14, p=0.0006, n=3) **(Fig. 3F)**. Collectively, PTX increases surface levels and polarization of peptide-bound MHCII, suggesting PTX-induced inflammation increases the likelihood that DRG neurons could activate $CD4^+$ T cells.

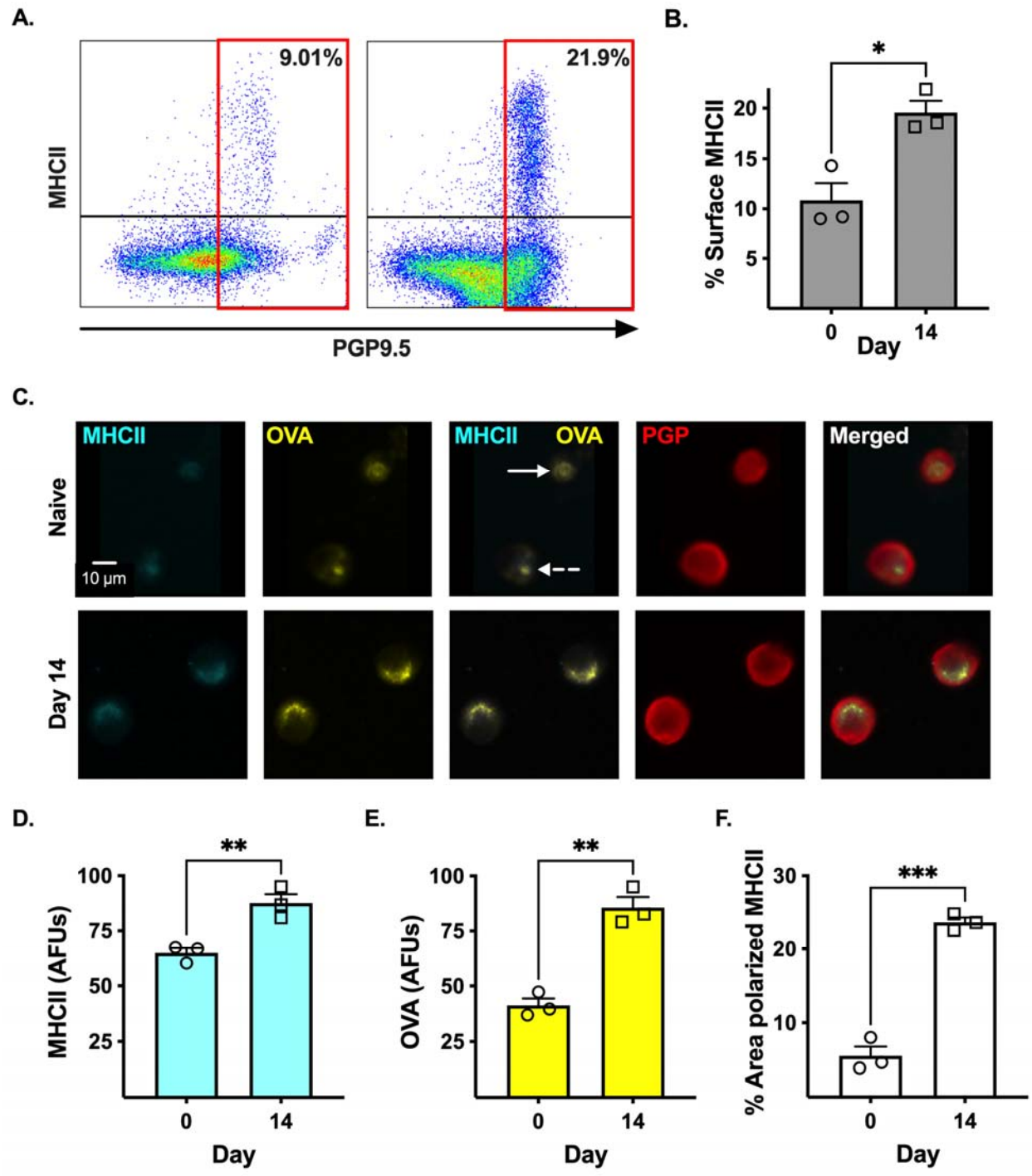

Fig. 3. MHCII presents peptide at the neuronal cell surface and expression increases after treatment with PTX. (A) Representative flow cytometric dot plots of the frequency of DRG neurons expressing surface-MHCII from naïve and day 14 PTX-treated female mice. **(B)** Quantification of the frequency of DRG neurons expressing surface-MHCII shown in **(A)**. **(C)** Representative widefield

fluorescence microscopy images of DRG neurons (PGP9.5^{+}: red) expressing surface-MHCII (cyan) co-localized with OVA-FITC (yellow) from naïve and day 14 PTX-treated female mice. Diffuse (solid arrow) and punctate (dashed arrow) surface-MHCII staining in DRG neurons from naïve female mice. Quantification of **(D)** MHCII intensity, **(E)** OVA intensity, and **(F)** percent of neuron area with polarized MHCII from **(C)**. Statistical significance determined by unpaired t-test (*p <0.05, **p < 0.01, ***p < 0.001, n=3/treatment).

MHCII protein is found in sensory neurons in mouse DRG tissue

MHCII protein was detected in mouse DRG neurons through immunohistochemistry (IHC) visualized by confocal **(Fig. 4A)** and widefield epifluorescence **(Fig. 4B)** microscopy. Confocal microscopy demonstrated that the MHCII signal was detected through the entire DRG neuron cell body **(Fig. 4A)**, excluding the possibility that the signal was originating from a proximal non-neuronal cell. DRG neurons from both naïve female and male mice expressed MHCII protein **(Fig. 4B, C,** 30.84% ± 6.37 in naïve female DRG and 46.64% ± 10.60 in naïve male DRG**)**. While PTX and inflammation induce the upregulation of MHCII on immune cells(*31*), the effect on neuronal MHCII is unknown. PTX increased the percent of MHCII^{+} DRG neurons in female mice from 30.84% ± 6.37 in naïve to 58.74% ± 7.69 14 days post-PTX **(Fig. 4B, C**, p=0.0190, n=8**)**. In contrast, the percent of MHCII^{+} neurons in male DRG did not increase significantly after administration of PTX **(Fig. 4B, C,** 46.64% ± 10.60 in naïve to 57.98% ± 7.01 14 days post-PTX**)**.

Reports suggest that MHCII molecules in endosomal MHC class II compartments (MIIC) are delivered to the plasma membrane as microclusters to enhance T cell recognition and signaling(*33*). Therefore, we quantified the number of MHCII microclusters (puncta) in DRG neurons from naïve and PTX-treated female and male mice. There were 7.61 ± 0.64 MHCII puncta/neuron in the DRG from naïve female

mice, which significantly increased to 12.84 ± 1.14 MHCII puncta/neuron 14 days post-PTX **(Fig. 4D**, p=0.0041, n=8**)**. In contrast, the number of MHCII puncta in DRG neurons from male mice remained constant after treatment with PTX (10.28 ± 1.60 in naïve to 12.32 ± 1.1 14 days post-PTX) **(Fig. 4D)**. In addition to the number of MHCII puncta, we measured the percent of neuronal cell area with MHCII puncta. The area with MHCII puncta on DRG neurons increased >2-fold in female mice 14 days post-PTX (2.01% ± 0.18 in naïve to 4.16% ± 0.54 14 days post-PTX, p=0.0024, n=8) **(Fig. 4E)**. In contrast, the area with MHCII puncta remained constant in DRG neurons from male mice (3.18% ± 0.67 in naïve to 3.90% ± 0.54 14 days post-PTX) **(Fig. 4D)**. Collectively, our data demonstrate that PTX treatment increases the expression of MHCII protein in DRG neurons only in female mice.

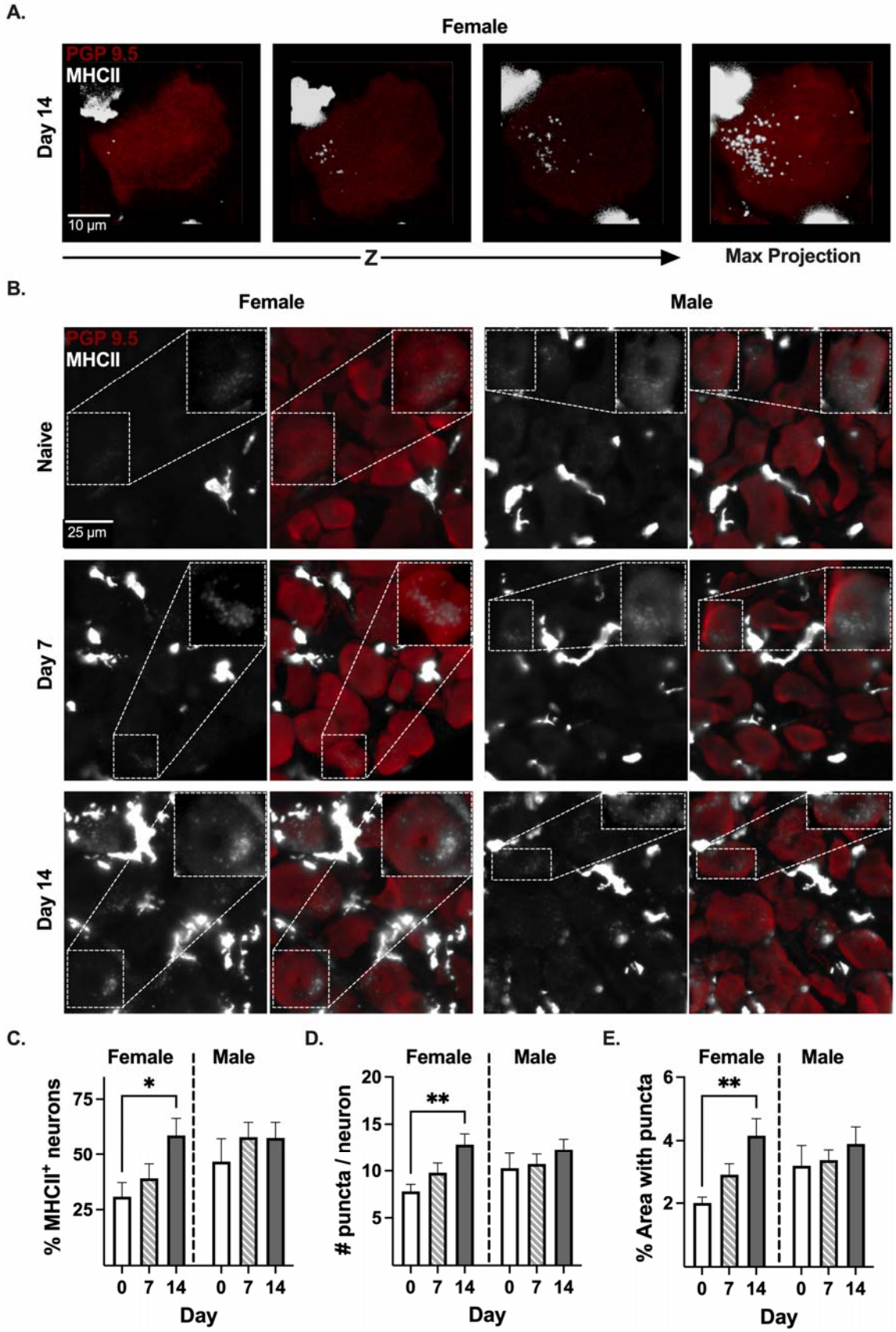
A.
Female
PGP 9.5
MHCII
Day 14
10 µm
Z
Max Projection
B.
Female
Male
PGP 9.5
MHCII
Naive
25 µm
Day 7
Day 14
C.
Female
Male
% MHCII+ neurons
75
50
25
*
0 7 14 0 7 14
Day
D.
Female
Male
puncta / neuron
20
15
10
5
**
0 7 14 0 7 14
Day
E.
Female
Male
% Area with puncta
6
4
2
**
0 7 14 0 7 14
Day

Fig.4. PTX increases neuronal MHCII in female DRG. (A) Representative confocal Z-stack and maximum projection IHC images of MHCII (grayscale) in PGP9.5^{+} (red) neuron in L4 DRG tissue from a day 14 PTX-treated female mouse. **(B)** Representative widefield epifluorescence images of DRG tissue from naïve and PTX-treated (day 7 and 14) female and male mice. Inset: representative MHCII^{+} neuron. Quantification of the **(C)** percent of MHCII^{+} neurons, **(D)** number of MHCII puncta/neuron, and **(E)** percent area with MHCII puncta from **(B)**. Statistical significance determined by 2-way ANOVA with Dunnett's multiple comparison test (*p <0.05, **p < 0.01, n=8/sex).

PTX induces the expression of MHCII protein in small diameter DRG neurons in female mice

PTX has been shown to affect both large (Aβ)(*34*) and small (A**δ** and C)(*34*) sensory nerve fibers at the peripheral terminals(*35*) and within the DRG(*8, 34*). Although low levels of MHCII transcript have been detected across all neuronal subsets in the DRG(*22*), it is unknown if the level of MHCII protein is dependent upon the diameter of the neuronal cell body. The diameter of neurons was calculated using an automated MetaXpress analysis pipeline and validated using DRG tissue from TRPV1-lineage td-tomato reporter mice **(Fig. S5)**. TRPV1 is a broad embryonic marker for many small diameter nociceptors including transient receptor potential cation channel subfamily V member (TRPV1), isolectin-B4 (IB4), and a subset of A**δ** neurons(*36*). Although MHCII protein was detected in large diameter neurons (>30µM(*37*)) in female naïve DRG tissue, the majority of MHCII^{+} neurons were small diameter (<25µM: 63.63% ± 3.056) **(Fig. 5A)**. After PTX treatment, the histogram of neuron diameter size of MHCII^{+} neurons shifted left toward the diameter mode of neurons from TRPV1-lineage td-tomato reporter mice **(Fig. 5A)**, indicating that PTX induced MHCII protein in small diameter neurons or reduced MHCII in large diameter neurons. The percent of small diameter neurons that were MHCII^{+} increased >2-fold after PTX treatment **(Fig. 5B,** 26.89% ± 5.48 in naïve to 55.37% ± 7.72 14 days post-PTX, p=0.0129, n=8**)** while the percent of large diameter neurons that were MHCII^{+} did not change **(Fig. S6**, 43.11% ± 9.23 in naïve to 67.81% ± 7.70 14 days post-PTX**),** indicating that PTX treatment induces MHCII expression in

small diameter neurons. Moreover, PTX treatment increased the number of MHCII puncta in small diameter neurons from 5.09 ± 0.45 puncta/neuron in naïve female DRG to 8.89 ± 0.87 puncta/neuron 14 days post-PTX **(Fig. 5C**, p=0.0022, n=8**)** and increased the percent of neuronal area with MHCII puncta >2-fold **(Fig. 5D,** 1.98% ± 0.21 in naïve to 4.08% ± 0.55 14 days post-PTX, p=0.0016, n=8**)**, further supporting induction of MHCII in small diameter neurons after treatment with PTX.

Similar to female mice, the majority of MHCII^{+} neurons in naïve male DRG were small diameter (<25µM: 66.00% ± 2.02) **(Fig. 5E)**. However, unlike females, the administration of PTX did not change the size distribution of MHCII^{+} DRG neurons **(Fig. 5E, red naïve line overlaps with blue day 14 PTX line)**. Therefore, not surprisingly, administration of PTX in male mice did not significantly change the percent of small **(Fig. 5F,** 43.86% ± 10.38 in naïve to 54.82% ± 6.90 14 days post-PTX**)** or large (**Fig. S6,** 55.27% ± 11.06 in naïve to 69.09% ± 7.41 14 days post-PTX**)** diameter neurons that were MHCII^{+}. Moreover, PTX did not change the number of puncta/neuron **(Fig. 5G)** or the percent of neuronal area with MHCII puncta **(Fig. 5H)**.

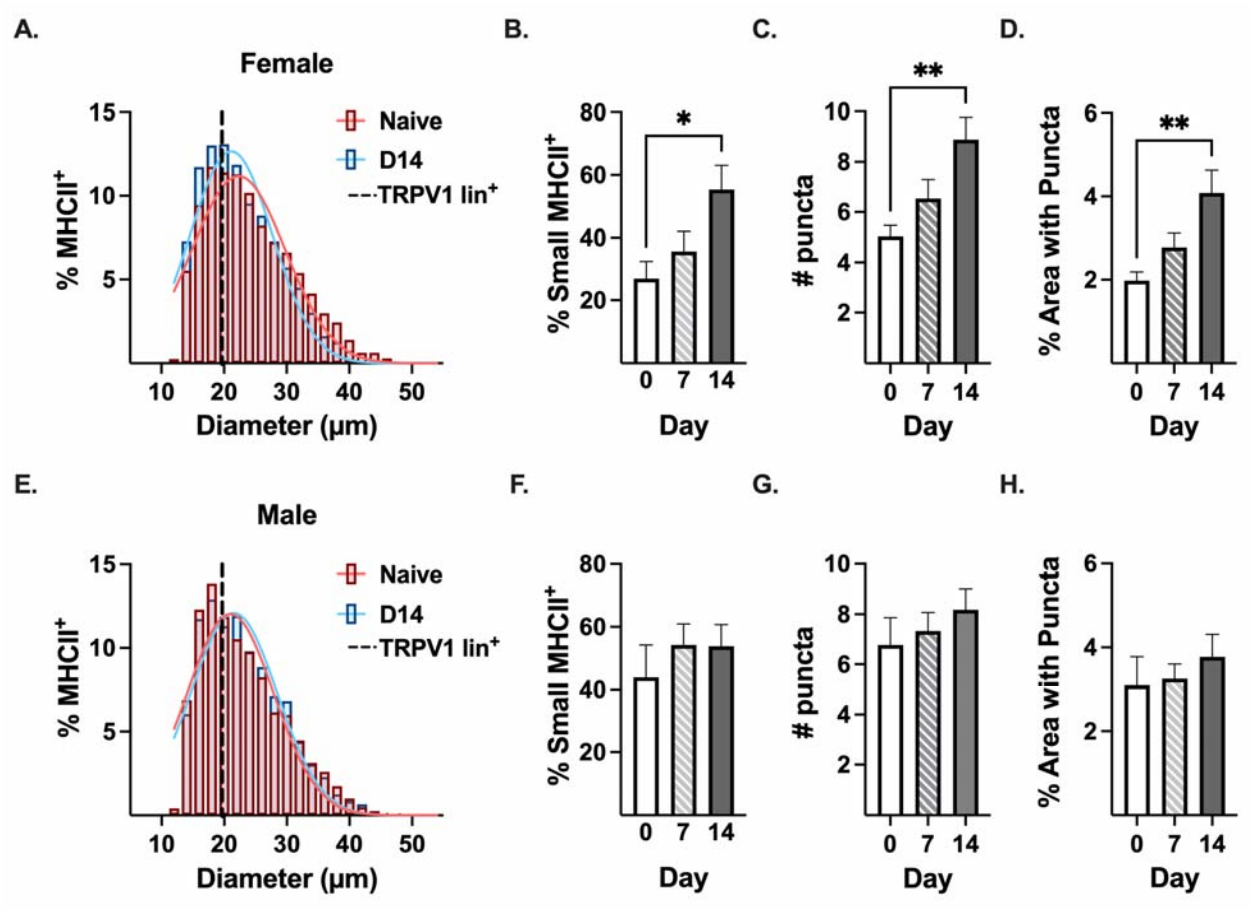

Fig. 5. MHCII$^+$ DRG neurons are primarily small diameter and expression increases after PTX. (A, E) Gaussian distribution of the diameter of MHCII$^+$ DRG neurons from naïve (red) and day 14 PTX-treated (blue) **(A)** female and **(E)** male mice (n=8/sex, pooled neurons). Dashed black line: diameter mode of td-tomato TRPV1-lineage neurons (Fig. S5). Quantification of **(B, F)** percent of small diameter (≤25 µm) MHCII$^+$ DRG neurons, **(C, G)** number of MHCII puncta/small diameter neuron, and **(D, H)** percent of small diameter neuron area with MHCII puncta. Statistical significance determined by 1-way ANOVA with Dunnett's multiple comparison test (*$p < 0.05$, **$p < 0.01$, n=8/sex).

Both nociceptive and non-nociceptive small diameter neurons express MHCII

Given the contribution of small nociceptive neurons to CIPN(*8*), and that the majority of MHCII is expressed in small diameter neurons, we knocked out MHCII in TRPV1-lineage neurons (**cHET:** TRPV1^{lin} MHCII$^{+/-}$ and **cKO:** TRPV1^{lin} MHCII$^{-/-}$). Knocking out MHCII in TRPV1-lineage neurons did not change the percent of small diameter MHCII^{+} neurons in the DRG of naïve female mice **(Fig. 6A)**. However, knocking out MHCII in TRPV1-lineage neurons prevented the PTX-induced increase in small diameter nociceptive DRG neurons in female mice 14 days post-PTX **(Fig. 6B)**. Knocking out one copy of MHCII in TRPV1-lineage neurons reduced the percent of PTX-induced small diameter MHCII^{+} neurons by almost 50% (55.37% ± 7.72 at day 14 in MHCII$^{+/+}$ to 33.30% ± 3.61 at day 14 in cHET, p-0.0342, n=8), while knocking out both copies of MHCII in TRPV1-lineage neurons reduced the percent of PTX-induced small diameter MHCII^{+} neurons by >75% (55.37% ± 7.72 at day 14 in MHCII$^{+/+}$ to 13.73% ± 1.54 at day 14 in cKO, p=0.0072, n=8 WT and n=2 cKO) **(Fig. 6C)**, further supporting that PTX induces MHCII in small diameter nociceptive DRG neurons. However, as TRPV1-lineage neurons comprise only 65% of small diameter neurons **(Fig. S5C)**, this indicates that the residual MHCII in small diameter neurons of cKO mice is a result of expression in a population of small non-nociceptive neurons in the DRG of both naïve and PTX-treated female mice.

In contrast to female mice, knocking out MHCII^{+} in TRPV1-lineage neurons in male mice reduced the percent of small diameter MHCII^{+} neurons by 66% in naïve cHET mice (43.86% ± 10.38 in MHCII$^{+/+}$ to 14.38% ± 3.18 in cHET, p=0.0063, n=8) and 87% in naïve cKO mice (43.86% ± 10.38 in MHCII$^{+/+}$ to 6.53% ± 0.70 in cKO, p=0.0215, n=8 WT and n=2 cKO) **(Fig. 6G)**. Likewise, knocking out MHCII^{+} in TRPV1-lineage neurons reduced the percent of small diameter MHCII^{+} neurons almost 50% in PTX-treated cHET male mice (53.82% ± 6.90 at day 14 in MHCII$^{+/+}$ to 29.09% ± 5.03 at day 14 in cHET, p=0.0378, n=8 WT) and 85% in PTX-treated cKO male mice (53.82% ± 6.90 at day 14 in MHCII$^{+/+}$ to 8.57% ± 0 at day 14 in cKO, n=2 cKO) **(Fig. 6G)**. Reduction of MHCII in conditional TRPV1-lineage

knockout mice further supports novel MHCII expression in DRG neurons from both sexes but regulation by PTX in only female mice.

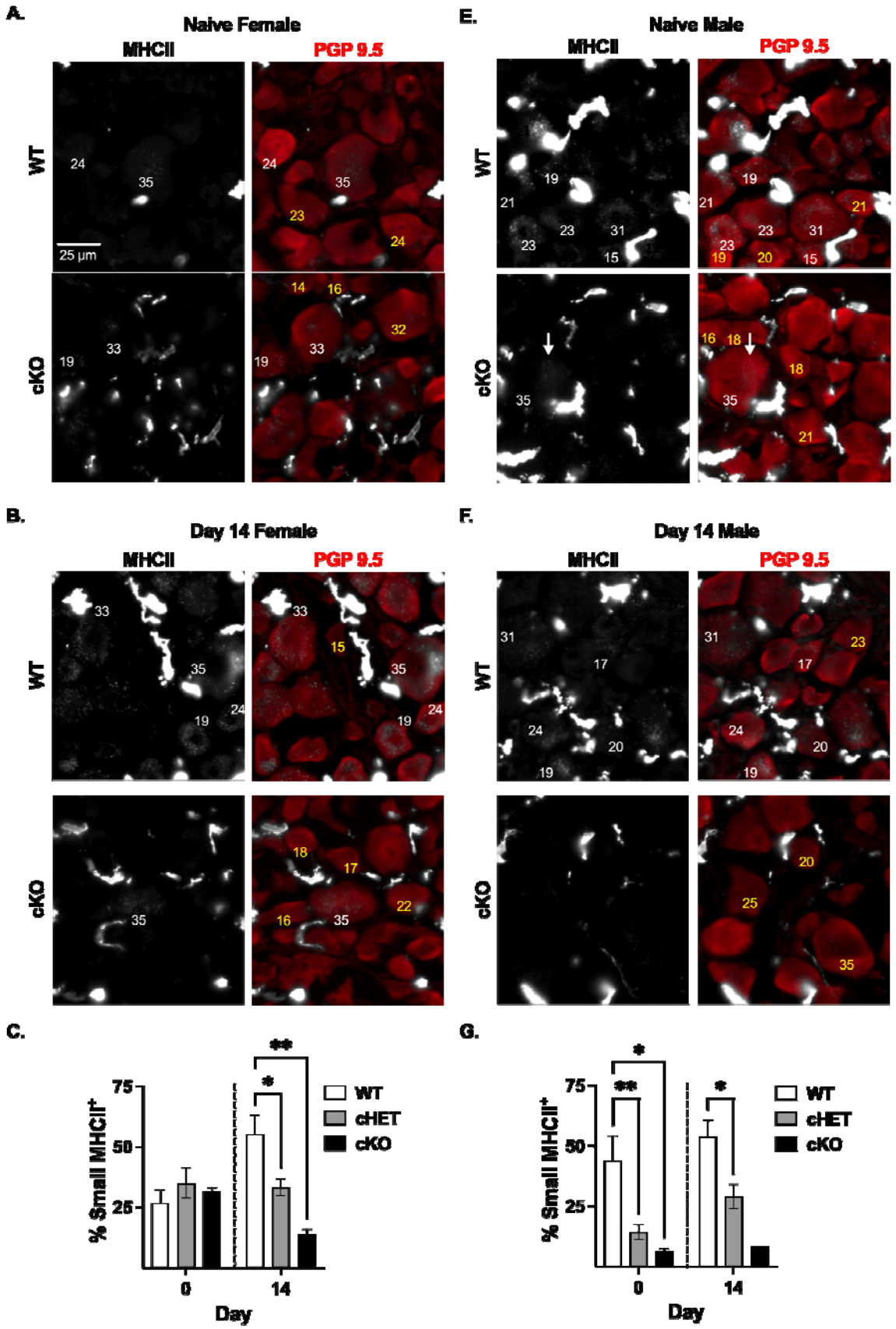
A.
Naive Female
MHCII
PGP 9.5
WT
cKO
25 µm
B.
Day 14 Female
MHCII
PGP 9.5
WT
cKO
C.
% Small MHCII+
75
50
25
0
14
Day
WT
cHET
cKO
E.
Naive Male
MHCII
PGP 9.5
WT
cKO
F.
Day 14 Male
MHCII
PGP 9.5
WT
cKO
G.
% Small MHCII+
75
50
25
0
14
Day
WT
cHET
cKO

Fig. 6. TRPV1-lineage neurons express MHCII in naïve male DRG and PTX treatment induces MHCII in TRPV1-lineage neurons in female DRG. (A-F) Immunohistochemistry of MHCII (grayscale) and neuronal marker PGP9.5 (red) in L4 DRG tissue from TRPV1-lineage $MHCII^{+/+}$ (WT), $MHCII^{+/-}$ (cHet) and $MHCII^{-/-}$ (cKO) naïve and day 14 PTX-treated female and male mice. Number = neuron diameter size, yellow ($MHCII^{+}$) and white ($MHCII^{-}$). Percent of small diameter $MHCII^{+}$ neurons for **(C)** female and **(G)** male WT, cHet, and cKO mice. Statistical significance determined by 2-way ANOVA with Dunnett's multiple comparison test (*p <0.05, **p <0.01; n=8 for WT and cHet; n=2 for male naïve, female naïve and day 14 cKO; n=1 for male day 14 cKO).

MHCII-expressing nociceptors attenuate cold hypersensitivity

As small diameter nociceptors contribute to CIPN(*8*) and cold hypersensitivity as one of the major symptoms(*38-40*), we tested the extent MHCII expressed in small nociceptive neurons protects against cold hypersensitivity assessed by the thermal placed preference (TPP) behavioral test. Although the mice are motivated to explore their environment, mice that are hypersensitive will avoid the cold plate and spend progressively less time on the cold plate as a result of learning from each successive trial.

As expected, knocking out MHCII in TRPV1-lineage neurons in naïve female mice did not induce cold hypersensitivity **(Fig. 7A)** as the majority of MHCII in the DRG of naïve female mice was expressed in small non-nociceptive neurons **(Fig. 5B)**. In contrast, knocking out MHCII in TRPV1-lineage neurons drastically increased cold hypersensitivity in naïve male mice **(Fig. 7B)**, which is consistent with MHCII being primarily expressed in small nociceptive neurons in naïve male mice **(Fig. 5F)**. With each successive trial, the TRPV1-lineage cHET male mice spent less time on the cold plate with a significant difference between trial 1 (49.52% ± 3.60) and trial 3 (18.45% ± 5.16, p=0.0004, n=12) but was not significantly different from wildtype (WT) mice until trial 4 (41.49% ± 7.738 for WT and 11.49% ± 5.00

for cHET, $p<0.0001$, n=12) **(Fig. 7B)**. This enhanced learning pattern to avoid the cold plate in cHET male mice indicates cold hypersensitivity, demonstrating that expression of MHCII in small nociceptive neurons prevents cold hypersensitivity in only naïve male mice.

Administration of PTX induced cold hypersensitivity in cHet female mice by trial 2 (51.87% ± 2.45 at trial 1 to 22.28% ± 3.58 at trial 2, $p<0.0001$, n=12), which was statistically more hypersensitive than WT female mice at trial 2 (37.16% ± 3.11 for WT and 22.28% ± 3.58 for cHET, $p=0.0493$, n=12) **(Fig. 7C)**. PTX-treated WT female mice were not hypersensitive to cold temperature until trial 3 (51.04% ± 1.77 at trial 1 to 26.27% ± 5.43 at trial 3, $p=0.0002$, n=12), further supporting that cHET female mice are more hypersensitive to cold temperature than WT female mice. Similar to female mice, PTX-treated cHET male mice were more hypersensitive to cold temperature than PTX-treated WT male mice. Administration of PTX induced cold hypersensitivity in cHET male mice at trial 2 (50.10% ± 2.21 at trial 1 to 22.17% ± 4.36 at trial 2 in in cHET, $p=0.0007$, n=12) and by trial 3 in WT male mice (50.69 ± 1.80 at trial 1 to 24.73 ± 6.18, $p=0.0007$, n=12)**(Fig. 7D)**; however, cHET male mice were only more hypersensitive to cold temperature compared to WT male mice at trial 3 (24.73% ± 6.18 for WT and 9.11% ± 3.67 for cHET, $p=0.0326$, n=12) **(Fig. 7D)**. Novel expression of MHCII in small diameter TRPV1-lineage nociceptors attenuates PTX-induced cold hypersensitivity in both female and male mice.

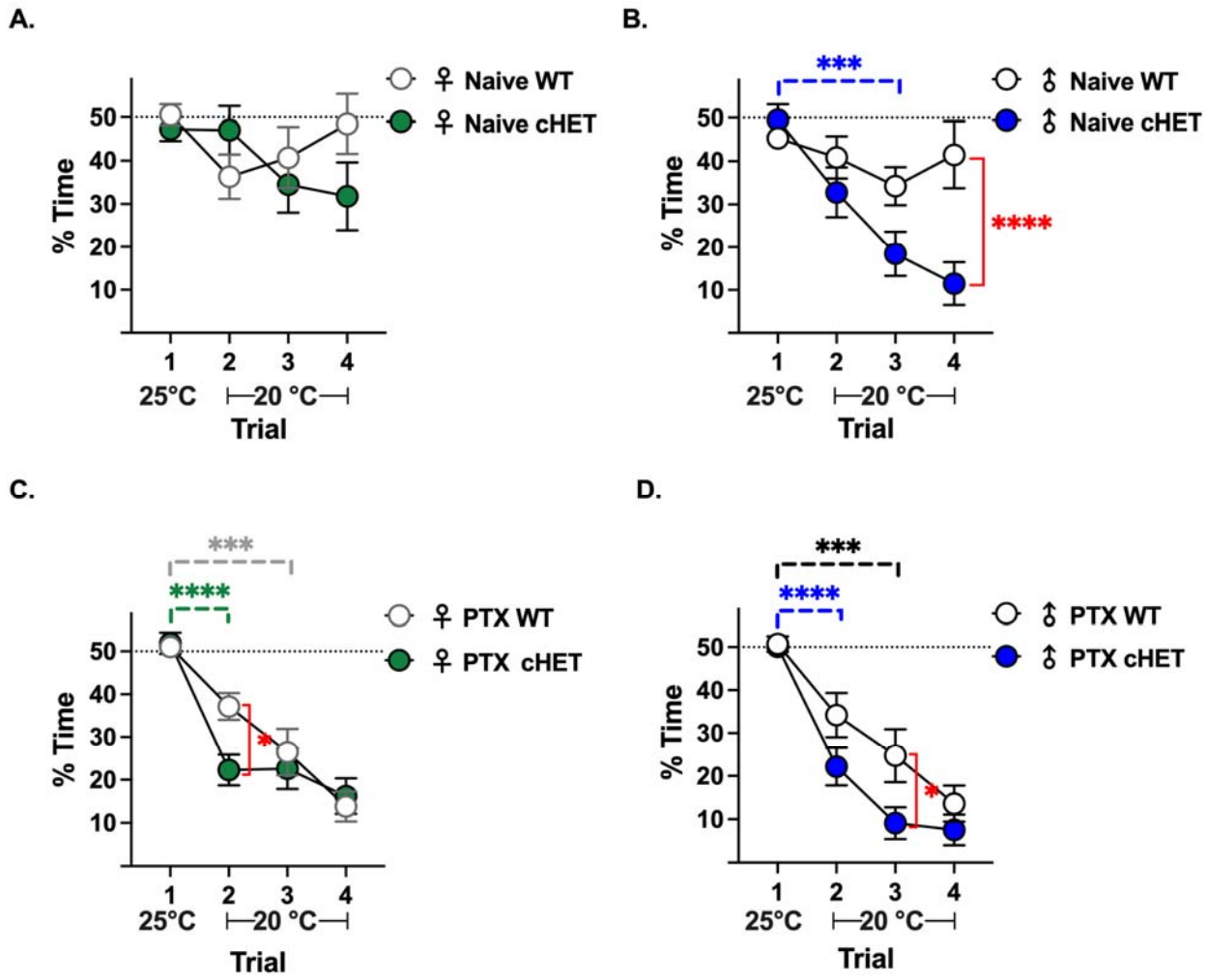

Fig. 7. MHCII in TRPV1-lineage neurons attenuates cold hypersensitivity. Thermal placed preference test (test plate = 25 °C, trial 1 and 20 °C, trials 2-4): Percent of time spent on test plate for **(A, B)** naïve and 6 days post-PTX **(C, D)** WT and cHET female and male mice. Dashed line: expected percent of time on test plate when mice not hypersensitive to cold. Statistical significance determined by 2-way ANOVA with Dunnett's multiple comparison test comparing trials 2-4 to trial 1 within same group (horizontal bars, complete statical analysis in **Table S1**), and Sidak's multiple tests for significance between groups at the same trial (red vertical bars) (*p <0.05, **p <0.01; ****p<0.0001 n=12/sex/group).

Model: Neuronal MHCII-dependent activation of CD4$^+$ T cells attenuates PTX-induced cold hypersensitivity in female and male mice

As the majority of CD4$^+$ T cells in the DRG are anti-inflammatory, we hypothesize that neuronal MHCII promotes activation of CD4$^+$ T cells to secrete anti-inflammatory cytokines that act directly on neurons to suppress hypersensitivity **(Fig. 8)**.

Naïve

Collectively, our data demonstrates that DRG neurons from naïve female and male mice express functional MHCII protein. Although large diameter neurons express MHCII, the majority of MHCII is present in small diameter neurons in DRG tissue of naïve female and male mice. Naïve female mice primarily express MHCII in small non-nociceptive neurons while naïve male mice primarily express MHCII in small nociceptive neurons. Building on our model from our previous publication, we hypothesize that MHCII on small non-nociceptive neurons and large diameter neurons maintains an anti-inflammatory environment by activating anti-inflammatory CD4$^+$ T cells (FoxP3 Tregs and IL-4)(*13*) in the DRG of female mice. Thus, knocking out MHCII in small nociceptive neurons in naïve female mice does not increase hypersensitivity to cold temperature. In contrast to female mice, MHCII on small nociceptive neurons in the DRG of male mice interacts with CD4$^+$ T cells to promote an anti-inflammatory environment through latency activated protein (LAP) and IL-10(*13*), which reduces hypersensitivity to cold temperature. Removal of MHCII on small nociceptive neurons decreases the anti-inflammatory environment making naïve cHET male mice more hypersensitive to cold temperature, as evidenced by a heighten avoidance response to the cold plate.

PTX

PTX binding directly to TLR-4 on DRG neurons and/or PTX-induced inflammation in the DRG of female mice induces MHCII on small diameter nociceptive neurons, which corresponds with a robust increase in anti-inflammatory $CD4^+$ T cells (FoxP3 Treg, IL-10, and IL-4)(*13*). The induction of MHCII on small nociceptive neurons in female DRG increases $MHCII^+$ neurons to the percent detected in male mouse DRG. Knocking out MHCII in TRPV1-lineage neurons reduces the percent or suppressive properties of anti-inflammatory $CD4^+$ T cells in the DRG, which exacerbates PTX-induced cold hypersensitivity in both female and male mice. Thus, MHCII in small nociceptive neurons attenuates PTX-induced cold hypersensitivity in both female and male mice.

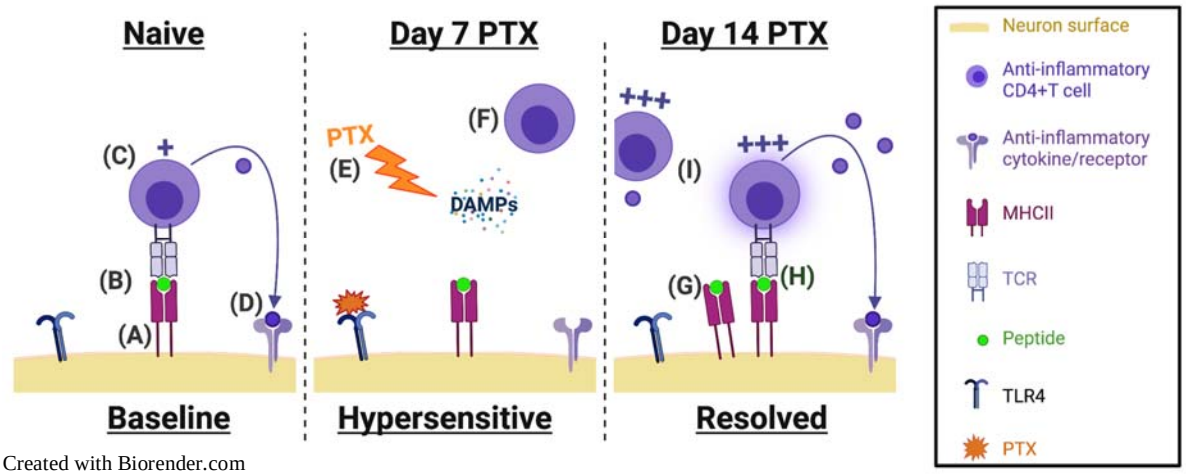

Created with Biorender.com

Fig. 8. Proposed model: Neuronal MHCII maintains homeostasis in the DRG and suppresses CIPN. **(A)** MHCII (magenta) on the surface of DRG neurons. **(B)** Presentation of peptide (green circle) bound to MHCII. **(C)** Neuronal MHCII-dependent activation of anti-inflammatory cytokine producing $CD4^+$ T cells (purple). **(D)** $CD4^+$ T cell cytokines binding to DRG neurons to maintain homeostasis. **(E)** CIPN due to PTX (orange polygon)-induced inflammation and/or PTX binding to neuronal TLR4 (blue). **(F)** Reduced $CD4^+$ T cell numbers and/or $CD4^+$ T cell dysfunction during peak hypersensitivity. **(G)** PTX-dependent induction of MHCII in small nociceptive neurons in the DRG of female mice. **(H)** $CD4^+$ T cell

receptor binding to peptide-MHCII to enhance $CD4^+$ T cell activation. **(I)** Increase in anti-inflammatory cytokine producing $CD4^+$ T cells during the resolution of CIPN.

DISCUSSION

The debilitating nature of CIPN has been a major obstacle for the continuation of life-saving measures for individuals with cancer. Recently, it has been shown that anti-inflammatory cytokines (IL-10 and IL-4) are protective against CIPN(*19, 41*); however, systemic use of IL-10 in general has had poor clinical outcomes(*42*) as it can promote the progression of cancer(*43*) and propagate chronic viral infections(*44*). In our recent work, we found that PTX induces a robust increase in anti-inflammatory $CD4^+$ T cells in the DRG of female mice (*13*), but the mechanism by which $CD4^+$ T cells are activated and the extent cytokines released by $CD4^+$ T cells target neurons in the DRG are unknown. We hypothesize that PTX exposure increases MHCII on sensory neurons to stimulate the paracrine release of anti-nociceptive cytokines by $CD4^+$ T cells to suppress CIPN.

By screening DRG neuron RNA seq data sets(*20-22, 30*), we found that mouse and human DRG neurons express transcripts for MHCII and MHCII-associated genes. MHCII is traditionally thought to be constitutively expressed only in APCs but can be induced by inflammation in non-APCs(*24*). To date, there are no reports that demonstrate MHCII protein expression in terminally differentiated neurons. Neuronal MHCII was most likely overlooked in the P. Hu et al. study as $MHCII^+$ cells in the DRG were identified based on morphology instead of co-staining with cell-specific markers. Additionally, the signal intensity of immune cell MHCII is >5 times greater than neuronal MHCII. Therefore, if not actively investigating neuronal MHCII, the settings used to capture immune cell MHCII would obscure neuronal MHCII. In addition, trying to identify a few molecules of MHCII is technically challenging as the signal

is not much higher than background. Thus, it is quite possible that neurons with extremely low level of MHCII were classified as negative cells in our study. Even though DRG neurons have fewer MHCII molecules than non-neuronal cells, it is likely still functionally significant given that clustering allows for as little as 210 MHCII molecules to activate a $CD4^+$ T cell(*45, 46*). Novel expression of MHCII in neurons will provide insight into the mechanism by which $CD4^+$ T cells contribute to pain, autoimmunity, and neurological diseases.

DRG neurons express RNA transcripts for chemokines CCL19/21/27(*30*), which are potent chemoattractants for $CD4^+$ T cells. Recently, CCL19/21 have been shown to induce the migration of $CD4^+$ T cells to non-lymphoid tissue, especially to the nervous system(*47, 48*), to preserve the balance between immune surveillance (against tumor and pathogens) and tolerance. The presence of $CD4^+$ T cells in naïve mouse DRG(*12, 13*), together with the expression of MHCII in neurons support direct cell-cell interaction, despite SGCs surrounding DRG neurons(*29*). Our present work demonstrates that $CD4^+$ T cells can breach the SGC barrier to directly contact DRG neurons. We predict that $CD4^+$ T cells transverse the SGC barrier in a manner similar to T cell diapedesis across endothelial cells to gain access to peripheral tissue. Likewise, $CD4^+$ T cells may attach to SGCs and crawl along until a permissive entrance site is reached, most likely a natural gap in the surrounding glial envelope or through a gap junction between adjacent glial cells. Direct $CD4^+$ T cell–neuron contact in the naïve mouse indicates a role for $CD4^+$ T cells in immune surveillance and tolerance. Therefore, we propose to expand the neuron-glial 2-cell unit into a 3-cell (neuron–$CD4^+$ T cell–glial) signaling complex that modulates neuronal function.

Nerve injury and nerve transection models demonstrate that macrophages can breach SGCs and lie directly against the neuron in the DRG(*26*) and trigeminal ganglion(*49*). Similarly, we found $CD4^+$ T cells in direct contact with DRG neurons after treatment with PTX. Moreover, the morphology of the $CD4^+$ T

cells in contact with DRG neurons were flattened on one side, which resembles the $CD4^+$ T cell shape that occurs during the formation of the immunological synapse (IS) with an APC(*50-52*). TCR signaling molecules accumulate at the flattened contact site resulting in an increase in calcium signaling, which is required to activate the T cell(*52*). Future studies are needed to determine whether DRG neurons form an IS with $CD4^+$ T cells to induce TCR signaling. Neuronal MHCII-dependent $CD4^+$ T cell activation would target cytokine release toward neurons to suppress hypersensitivity after inflammation and/or nerve injury.

Regulation of neuronal MHCII is most likely dependent upon specific nerve injury and/or inflammatory conditions (i.e., nerve transection vs CIPN). In the case of non-infectious nerve injury/inflammation (i.e., CIPN), we hypothesize that DRG neurons present self-peptides on MHCII to initiate an anti-inflammatory $CD4^+$ T cell response. Although SGCs can secrete anti-inflammatory cytokines(*53, 54*), antigen-specific $CD4^+$ T cell activation is advantageous as cytokine release would be more tightly regulated. Therefore, depending on the particular condition, antigen-specific $CD4^+$ T cells could impact the function of distinct subsets of neurons instead of modulating neuronal function in a global, non-specific manner. Future studies will investigate which self-peptides may be driving neuron-dependent $CD4^+$ T cell responses.

The synthesis and trafficking of MHCII molecules is dependent upon the cell type and activation status(*32, 55, 56*). Although the common function for $MHCII^+$ cells is to present antigen to $CD4^+$ T cells, the cell specific differences in MHCII processing and presentation dictate cell-specific roles in the immune response(*57*). In naïve DCs and macrophages, MHCII molecules are found within late endosomal MIIC with some cell-surface expression(*55, 56*), while B cells have very little MHCII in late endosomal MIIC but have the majority on the cell surface and in early endosomes(*58*). We found that naïve DRG neurons primarily express intracellular MHCII puncta, suggesting endosomal MIIC, but

future studies are required to determine the exact intracellular location within the MHCII processing pathway. Trafficking of MHCII from intracellular compartments to the plasma membrane typically increases after DC activation in response to cytokines or triggering of pattern recognition receptors (PRRs)(*59*). DRG neurons express transcripts and/or protein for many PRRs, including TLR 1-9(*30, 60-64*) with female mice having >5-fold more TLR4-6 transcripts than male mice(*30*). Accordingly, neuronal TLR4 signaling in DRG neurons mediates mechanical hypersensitivity after a nerve injury in only female mice(*65*). Similarly, we found that PTX, which binds to TLR4, increases MHCII in DRG neurons of only female mice, further supporting a sex-specific role for TLR4 in the DRG.

Small diameter neurons, which consist of A□ and unmyelinated C-fibers, have also been shown to contribute to CIPN(*8*). C-fibers can be further subdivided into nociceptive TRPV1 and IB4 neurons, which respond to noxious stimuli, and non-nociceptive **l**ow **t**hreshold **m**echano**r**eceptors (C-LTMRs: majority tyrosine hydroxylase (TH) neurons and minority mas-related G-protein receptor B4 (MrgB4) neurons). As cold hypersensitivity is a major symptom of CIPN(*38-40*), we assessed the contribution of MHCII in small diameter nociceptive neurons by TPP. TPP is a behavioral test that incorporates the ability to choose and the potential to learn, demonstrating higher order pain processing. We found that reducing the expression of MHCII in TRPV1-lineage neurons in naive male and female mice induced cold hypersensitivity in only male mice. Therefore, the majority of MHCII^{+} neurons in the DRG of naïve female mice were not TRPV1-lineage neurons but non-nociceptive C-LTMRs. Although C-LTMRs typically process innocuous gentle and affective touch, there are a few reports that indicate a role for TH neurons in pain(*66, 67*), suggesting that either MHCII in TH neurons protects against cold hypersensitivity or that neuronal MHCII does not contribute to cold hypersensitivity in naïve female mice.

Administration of PTX induces MHCII in C-nociceptive neurons in female mice, so reducing the expression of MHCII in TRPV1-lineage neurons exacerbates PTX-induced cold hypersensitivity in both male and female mice. In addition to TRPV1-lineage neurons, we found in both female and male mice that MHCII is expressed in large diameter neurons, which primarily convey non-nociceptive input (proprioception, touch, pressure, vibration) from the periphery to the spinal cord but may contribute to nociceptive circuits following tissue or nerve injury as in CIPN(*34*). MHCII expression in small and large LTMRs indicates that PTX-induced cold hypersensitivity may be even greater if MHCII is eliminated from all neurons and also suggests a role in proprioception, pressure, and touch (light, gentle and affective). Future studies will address the role of MHCII in large and small diameter LTMRs in pain and other sensory modalities.

We predict that neuronal MHCII is protective in acute CIPN by inducing anti-inflammatory $CD4^+$ T cells in the DRG, but chronic CIPN may result due to a break in tolerance. Although the source of MHCII peptides is generally thought to be exogenous, 25-55% of MHCII peptides are derived from cytosolic and nuclear proteins(*68, 69*), presumably through autophagic processes(*70*). Autophagy, a critical pathway in terminally differentiated neurons(*71*), may be the prime source of MHCII peptides in DRG neurons. The majority of MHCII peptides during inflammation and infection have been shown to be self(*72-74*), indicating an important role for anti-inflammatory $CD4^+$ T cells to suppress self-reactivity and preserve tolerance. However, chronic and uncontrolled inflammatory conditions may lead to a loss of tolerance, which likely occurs for individuals who develop chronic CIPN.

Understanding the endogenous $CD4^+$ T cell response in the DRG will provide novel targets to activate a specific subpopulation of neuroprotective $CD4^+$ T cells to suppress the inflammatory response in the DRG after PTX administration. Targeting neuron-specific $CD4^+$ T cells should not compromise the pro-inflammatory immune response that is required to kill the cancer cells. Neuronal MHCII represents a

novel mechanism to suppress CIPN, which could be exploited for therapeutic intervention against not only pain but autoimmunity and neurological diseases.

MATERIALS AND METHODS

Study Design

The objectives of this study were to determine whether $CD4^+$ T cells directly contact DRG neurons and identify immune molecules expressed in DRG neurons that facilitate direct cell-cell communication with $CD4^+$ T cells. After identifying MHCII in DRG neurons, our third objective was to determine the functional impact of neuronal MHCII on cold hypersensitivity in the well-established PTX-induced peripheral neuropathy mouse model(*75*). Our experimental approach included molecular and immunochemical assays, flow cytometry, targeted manipulation of gene expression, and behavioral tests using male and female mice. Immunochemical analysis was performed manually by two independent blinded experimenters and by using an automated MetaXpress pipeline to eliminate human bias. All mouse experiments were randomly assigned a treatment, which experimenters were blinded to.

Mice

Male and female mice were purchased from Jackson Laboratory **(Table S2)**. Male $TRPV1^{Cre}$ mice were bred to female $MHCII^{fl/fl}$ mice to generate $TRPV1^{lin}$ $MHCII^{+/-}$ heterozygote mice **(cHET)**. cHET female mice were mated back to $MHCII^{fl/fl}$ male mice to delete MHCII from TPRV1-lineage nociceptors, which includes IB4, TRPV1, and a subset of A□ neurons ($TRPV1^{lin}$ $MHCII^{-/-}$ mice; **cKO**). To confirm the presence of $MHCII^{fl/fl}$ and Cre, mouse tails were digested with 50mM NaOH/50mM HCl/1M Tris-HCl, pH 8.0. Primers (Table S3) and Promega GoTaq® G2 Hot Start Polymerase were used in PCR to detect

MHCII$^{fl/fl}$ (199 base pair), MHCII$^{fl/+}$ (199 and 295 base pairs), and wild type MHCII$^{+/+}$ (295 base pair) mice. PCR using GoTaq® Polymerase determined the presence of Cre **(Table S3)**. cHET×MHCII$^{fl/fl}$ crosses only yielded 8% cKO mice (4% per sex) instead of the predicted 25% (12.5% per sex) based on normal Mendelian genetics. cKO mice were used to validate MHCII protein in small nociceptive neurons.

All mice were given food and water *ad libitum*. All experimental protocols followed National Institutes of Health guidelines and were approved by the University of New England Institutional Animal Use and Care Committee. Mice were euthanized with an overdose of avertin (0.5cc of 20 mg/ml) followed by transcardiac perfusion with 1× phosphate buffered saline (PBS). This method of euthanasia is consistent with American Veterinary Medical Association Guidelines for the Euthanasia of Animals.

Paclitaxel and Thermal Placed Preference test (TPP)

PTX (Sigma-Aldrich) was solubilized in cremophor:ethanol 1:1 and diluted 1/3 in 1× PBS. A single injection of 6mg/kg PTX at a volume of 10ml/kg bodyweight was given on day 0 as done previously(*12, 13*). The TPP test was used to quantify non-evoked measures of cold hypersensitivity before and after PTX. Mice were habituated to the room and testing apparatus, which includes two adjustable thermal plates (test and reference). Mice were placed on the reference plate to begin each 3-minute trial. The reference plate side was the same for all trials for an individual mouse, but the sides for the reference and test plates were counterbalanced within each group to exclude a potential side preference. For the habituation trial (#1), both the test and reference plates were set to 25 °C, and the mice were allowed to explore for 3 minutes. Any mouse that spent <30 seconds on the test plate during the habituation trial was excluded from further testing. For trials #2-4, the reference plate was set to 25 °C and the test plate to 20 °C. The percent of time the mice spent on the test plate was reported for each trial. Separate cohorts of

mice were run for naive and 6 days post-PTX to prevent confounding effects of avoidance learning during the naive session impacting the day 6 results.

Immunohistochemistry

Mice were perfused with 1× PBS followed by 4% paraformaldehyde (PFA; Sigma-Aldrich). L4 DRGs were post-fixed in 4% PFA for 1-2 hours, then transferred to 30% sucrose/0.02% sodium azide at 4 °C. DRGs were embedded in Clear Frozen Selection Compound prior to serially sectioning at 12 µm slices. DRGs were permeabilized with 1× PBS/0.1% Triton X-100 (PBS-T; Sigma-Aldrich) for 15 minutes at room temperature (RT) and incubated with blocking buffer (PBS-T plus 5% normal donkey serum) for 1 hour at RT.

Slides were incubated with primary antibodies **(Table S4)** in blocking buffer overnight at RT in a humidified, light-protected chamber. Slides were washed 3X with 1× PBS and secondary antibodies **(Table S4)** added for 1 hour at RT. Slides were washed 3X with 1× PBS, then cover slipped with Fluoroshield Mounting Medium (±DAPI, Abcam). $CD4^+$ T cell–DRG neuron images were acquired with a 40× objective (HC PL Fluotar NA 0.60 with correction ring; Z-stacks with 1 µm step) on an ImageXpress Pico automated widefield fluorescence microscope from Molecular Devices, software version 2.9.3. All other images were acquired with a 40× objective (Plan Fluor NA 0.75) on a Keyence BZ-X710 automated widefield fluorescence microscope. Keyence images were imported into Fiji(*76*) to generate single channel images, then analyzed by MetaXpress software for percent $MHCII^+$ neurons, $MHCII^+$ neuron diameter, and number and area of neuron with MHCII puncta **(Supplemental methods).**

Immunocytochemistry

DRGs were pooled for each mouse and acutely dissociated into a single cell suspension as described previously(*13*). DRG neurons were isolated by depleting non-neuronal cells through MACS following the manufacturer's protocol (Miltenyi). MACS-DRG neurons were resuspended in F12 media supplemented with 10% fetal bovine serum (FBS) and 100 µg/ml primocin (Invivogen) and plated on chamber slides (Millipore) coated with 20 µg/ml laminin (Sigma) and 50 µg/ml poly-D-lysine (Thermo).

Total MHCII

After an 18-hour incubation at 37 °C, MACS-neurons were washed with 1× PBS and fixed with 4% PFA. Cells were washed with 1× PBS and incubated with blocking buffer for 30 minutes at RT. PGP9.5 was added to the cells for 1 hour at RT. Cells were washed with 1× PBS and incubated with anti-rabbit 488 secondary antibody and MHCII for 1 hour at RT. Slides were imaged with a Leica TCS SP5 II confocal microscope using a 40× objective under oil.

Extracellular MHCII and OVA peptide

After an 18-hour incubation at 37 °C, media was replaced with F12/10% FBS/100 µg/ml primocin. FITC-conjugated OVA peptide (Anaspec) was added at 10 µg/ml for 30 minutes at 37 °C. Cells were washed with 1× PBS/1% FBS and blocked with CD16/32 (Biolegend). After 10 minutes, cells were incubated with MHCII for 30 minutes on ice to stain for extracellular MHCII. Cells were washed, fixed with 4% PFA, and stained with PGP9.5. Slides were imaged on the Keyence microscope with a 20× objective. MetaXpress software was used to analyze surface-MHCII and OVA MPI, and the percent neuron area with polarized MHCII **(Supplemental methods)**.

Flow cytometry

DRG cells from naïve and day 14 PTX-treated female mice were incubated at RT for 30 min with Live/Dead Fixable Violet (Thermo). Cells were pre-incubated with CD16/32 for 10 min prior to the addition of MHCII or isotype for 20 min at 4 °C. Cells were washed with FACs buffer (1× PBS, 1% FBS) and fixed at RT for 20 min with Intracellular Staining Fixation Buffer (BioLegend). Cells were washed with 2× Cyto-FastTM Perm Wash solution (CFPWS; BioLegend) and incubated with PGP9.5 for 20 min at RT. Cells were washed with 2× CFPWS and incubated with donkey anti-rabbit Cy3 for 20 min at RT. VersaComp Antibody Capture Kit (Beckman Coulter) was used to set compensation to correct for spectral overlap. Unstained DRG cells were used to check for auto-fluorescence. Beckman Coulter Cyto-FLEX S System B2-R3-V4-Y4 was used to acquire >10,000 events in the live PGP9.5 DRG neuron gate. Data was analyzed with FlowJo™ 10.8.2.

Western blot

MACS-DRG neurons from naïve and day 14 PTX-treated female mice were lysed in DiGE lysis buffer (7 M urea, 2 M thiourea, 4% CHAPS, 30 mM Tris-HCl) supplemented with 1× Halt Protease and Phosphatase Inhibitor Cocktail (Thermo). Lysates were quantified with the EZQ Protein Quantification Kit (Thermo). Lysates (20 μg) were added to Bolt bis-Tris 12 % gel (Thermo). SDS-PAGE was performed using 1× MOPS SDS Running Buffer (Life Technologies). Proteins were transferred to Immobilon-FL PVDF membrane (Millipore) using 1× Power Blotter 1-Step Transfer Buffer (Invitrogen). PVDF membranes were incubated at 4 °C for 48 hours with MHCII and beta tubulin as the loading control, then incubated with 1:2000 donkey anti-rabbit Cy5 secondary antibody for 2 hours at RT. PVDF membranes were imaged using the Typhoon 9600 laser scanner (GE). Band intensities were quantified using AutoQuant imaging software.

Statistical Analysis

All experiments were analyzed using Graphpad Prism 9 (Graphpad Software, Inc) and reported as mean ± standard error of mean. An arcsine transformation was performed on all percentage data prior to statistical analysis. For western blot, ICC, and flow cytometry, an unpaired t-test was used to compare the means of neuronal MHCII from naïve and day 14 PTX-treated mice (**Figs. 2, 3**). A two-way ANOVA with Dunnett's multiple comparison test was used to compare the means of MHCII for PTX-treated (day 7 and 14) male and female mice to the naïve control (**Fig. S2, Figs. 4 and 6**). TPP behavior was analyzed using a two-way ANOVA with Dunnett's multiple comparison test comparing the mean percent of time on the cold plate (trials #2-4) to the control (#1) within the same group. Sidak multiple comparison test was used to compare the means between two groups within the same trial.

Supplementary Materials

Materials and Methods

Tables

Table S1. Two-way ANOVA analysis with Dunnett's multiple comparison test for PTX-treated female and male WT and cHET for TPP test shown in **Fig. 7**.

Table S2. Jackson Laboratory mouse strains used in the study.

Table S3. Primer sequences for TRPV-1 lineage MHCII conditional knockout mice.

Table S4. Antibody details for each application.

Figures

Fig. S1. $CD4^+$ T cells directly contact neurons in female mouse DRG tissue.

Fig. S2. DRG neurons from human and mouse express transcripts for MHCII and MHCII-associated genes.

Fig. S3. DRG neurons from naive female and male mice express nuclear RFX1 protein.

Fig. S4. $PGP9.5^+$ neurons comprise a fraction of total DRG cells.

Fig. S5. High throughput automated image analysis module identifies small and large diameter neurons in female and male DRG tissue.

Fig. S6. PTX does not change the percent of large diameter neurons that express MHCII in male and female DRG.

References

1. B. A. Weaver, How Taxol/paclitaxel kills cancer cells. *Mol Biol Cell* **25**, 2677-2681 (2014).
2. M. Seretny *et al.*, Incidence, prevalence, and predictors of chemotherapy-induced peripheral neuropathy: A systematic review and meta-analysis. *Pain* **155**, 2461-2470 (2014).
3. J. M. Jimenez-Andrade *et al.*, Vascularization of the dorsal root ganglia and peripheral nerve of the mouse: implications for chemical-induced peripheral sensory neuropathies. *Mol Pain* **4**, 10 (2008).
4. H. Hirakawa *et al.*, Regional differences in blood-nerve barrier function and tight-junction protein expression within the rat dorsal root ganglion. *Neuroreport* **15**, 405-408 (2004).
5. C. A. Byrd-Leifer, E. F. Block, K. Takeda, S. Akira, A. Ding, The role of MyD88 and TLR4 in the LPS-mimetic activity of Taxol. *Eur J Immunol* **31**, 2448-2457 (2001).
6. Y. Li *et al.*, DRG Voltage-Gated Sodium Channel 1.7 Is Upregulated in Paclitaxel-Induced Neuropathy in Rats and in Humans with Neuropathic Pain. *J Neurosci* **38**, 1124-1136 (2018).
7. W. Boehmerle *et al.*, Paclitaxel induces calcium oscillations via an inositol 1,4,5-trisphosphate receptor and neuronal calcium sensor 1-dependent mechanism. *Proc Natl Acad Sci USA* **103**, 18356 (2006).
8. Y. Li *et al.*, Dorsal root ganglion neurons become hyperexcitable and increase expression of voltage-gated T-type calcium channels (Cav3.2) in paclitaxel-induced peripheral neuropathy. *Pain* **158**, (2017).
9. Y. Goshima *et al.*, Computational analysis of the effects of antineoplastic agents on axonal transport. *J Pharmacol Sci* **114**, 168-179 (2010).
10. S. J. L. Flatters, G. J. Bennett, Studies of peripheral sensory nerves in paclitaxel-induced painful peripheral neuropathy: Evidence for mitochondrial dysfunction. *Pain* **122**, 245-257 (2006).
11. E. K. Rowinsky, E. A. Eisenhauer, V. Chaudhry, S. G. Arbuck, R. C. Donehower, Clinical toxicities encountered with paclitaxel (Taxol). *Semin Oncol* **20**, 1-15 (1993).
12. X.-J. Liu *et al.*, Nociceptive neurons regulate innate and adaptive immunity and neuropathic pain through MyD88 adapter. *Cell Res* **24**, 1374-1377 (2014).
13. D. J. Goode, E. E. Whitaker, N. E. Mecum, Ovariectomy increases paclitaxel-induced mechanical hypersensitivity and reduces anti-inflammatory CD4+ T cells in the dorsal root ganglion of female mice. *Journal of Neuroimmunology*, 577878 (2022).
14. S. L. Klein, K. L. Flanagan, Sex differences in immune responses. *Nature Reviews Immunology* **16**, 626-638 (2016).
15. J. C. Copray *et al.*, Expression of interleukin-1 beta in rat dorsal root ganglia. *J Neuroimmunol* **118**, 203-211 (2001).
16. F. Wang, I. Millet, K. Bottomly, A. Vignery, Calcitonin gene-related peptide inhibits interleukin 2 production by murine T lymphocytes. *J Biol Chem* **267**, 21052-21057 (1992).
17. F. Richter *et al.*, Interleukin-17 sensitizes joint nociceptors to mechanical stimuli and contributes to arthritic pain through neuronal interleukin-17 receptors in rodents. *Arthritis Rheum* **64**, 4125-4134 (2012).
18. K. S. Vikman, R. H. Hill, E. Backström, B. Robertson, K. Kristensson, Interferon-γ induces characteristics of central sensitization in spinal dorsal horn neurons in vitro. *Pain* **106**, 241-251 (2003).
19. K. Krukowski *et al.*, CD8+ T Cells and Endogenous IL-10 Are Required for Resolution of Chemotherapy-Induced Neuropathic Pain. *J Neurosci* **36**, 11074-11083 (2016).
20. M. Q. Nguyen, L. J. von Buchholtz, A. N. Reker, N. J. P. Ryba, S. Davidson, Single-nucleus transcriptomic analysis of human dorsal root ganglion neurons. *eLife* **10**, e71752 (2021).
21. D. Tavares-Ferreira *et al.*, Spatial transcriptomics of dorsal root ganglia identifies molecular signatures of human nociceptors. *Sci Transl Med* **14**, eabj8186 (2022).
22. D. Usoskin *et al.*, Unbiased classification of sensory neuron types by large-scale single-cell RNA sequencing. *Nat Neurosci* **18**, 145-153 (2015).
23. P. Ray *et al.*, Comparative transcriptome profiling of the human and mouse dorsal root ganglia: an. *Pain* **159**, 1325-1345 (2018).
24. M. van Velzen *et al.*, Neuron-Interacting Satellite Glial Cells in Human Trigeminal Ganglia Have an APC Phenotype. *J. Immunol.* **183**, 2456 (2009).
25. B. Vagaska *et al.*, MHC-class-II are expressed in a subpopulation of human neural stem cells in vitro in an IFNγ–independent fashion and during development. *Scientific Reports* **6**, 24251 (2016).
26. P. Hu, E. M. McLachlan, Macrophage and lymphocyte invasion of dorsal root ganglia after peripheral nerve lesions in the rat. *Neuroscience* **112**, 23-38 (2002).

27. G. Laumet *et al.*, Interleukin-10 resolves pain hypersensitivity induced by cisplatin by reversing sensory neuron hyperexcitability. *Pain*, (2020).
28. X. Chen *et al.*, Deficiency of anti-inflammatory cytokine IL-4 leads to neural hyperexcitability and aggravates cerebral ischemia–reperfusion injury. *Acta Pharmaceutica Sinica B*, (2020).
29. J. S. Dixon, Changes in the fine structure of satellite cells surrounding chromatolytic neurons. *The Anatomical Record* **163**, 101-109 (1969).
30. D. M. Lopes, F. Denk, S. B. McMahon, The Molecular Fingerprint of Dorsal Root and Trigeminal Ganglion Neurons. *Frontiers in Molecular Neuroscience* **10**, (2017).
31. L. W. Pfannenstiel, S. S. Lam, L. A. Emens, E. M. Jaffee, T. D. Armstrong, Paclitaxel enhances early dendritic cell maturation and function through TLR4 signaling in mice. *Cell Immunol* **263**, 79-87 (2010).
32. M. Cella, A. Engering, V. Pinet, J. Pieters, A. Lanzavecchia, Inflammatory stimuli induce accumulation of MHC class II complexes on dendritic cells. *Nature* **388**, 782-787 (1997).
33. B. Bosch, E. L. Heipertz, J. R. Drake, P. A. Roche, Major histocompatibility complex (MHC) class II-peptide complexes arrive at the plasma membrane in cholesterol-rich microclusters. *J Biol Chem* **288**, 13236-13242 (2013).
34. H. Zhang, P. M. Dougherty, Enhanced excitability of primary sensory neurons and altered gene expression of neuronal ion channels in dorsal root ganglion in paclitaxel-induced peripheral neuropathy. *Anesthesiology* **120**, 1463-1475 (2014).
35. C. Siau, W. Xiao, G. J. Bennett, Paclitaxel- and vincristine-evoked painful peripheral neuropathies: loss of epidermal innervation and activation of Langerhans cells. *Exp Neurol* **201**, 507-514 (2006).
36. M. J. Patil, A. H. Hovhannisyan, A. N. Akopian, Characteristics of sensory neuronal groups in CGRP-cre-ER reporter mice: Comparison to Nav1.8-cre, TRPV1-cre and TRPV1-GFP mouse lines. *PLOS ONE* **13**, e0198601-e0198601 (2018).
37. C. Ho, J. Zhao, S. Malinowski, M. Chahine, M. E. O'Leary, Differential Expression of Sodium Channel β Subunits in Dorsal Root Ganglion Sensory Neurons*. *Journal of Biological Chemistry* **287**, 15044-15053 (2012).
38. X. Luo *et al.*, Macrophage Toll-like Receptor 9 Contributes to Chemotherapy-Induced Neuropathic Pain in Male Mice. *The Journal of Neuroscience* **39**, 6848-6864 (2019).
39. R. C. Polomano, A. J. Mannes, U. S. Clark, G. J. Bennett, A painful peripheral neuropathy in the rat produced by the chemotherapeutic drug, paclitaxel. *Pain* **94**, 293-304 (2001).
40. S. B. Smith, S. E. Crager, J. S. Mogil, Paclitaxel-induced neuropathic hypersensitivity in mice: responses in 10 inbred mouse strains. *Life Sci* **74**, 2593-2604 (2004).
41. Q. Shi *et al.*, Interleukin-4 protects from chemotherapy-induced peripheral neuropathy in mice modal via the stimulation of IL-4/STAT6 signaling. *Acta Cir Bras* **33**, 491-498 (2018).
42. A. Saxena *et al.*, Interleukin-10 paradox: A potent immunoregulatory cytokine that has been difficult to harness for immunotherapy. *Cytokine* **74**, 27-34 (2015).
43. E. Lech-Maranda *et al.*, Elevated IL-10 plasma levels correlate with poor prognosis in diffuse large B-cell lymphoma. *Eur Cytokine Netw* **17**, 60-66 (2006).
44. D. R. Nelson *et al.*, Long-term interleukin 10 therapy in chronic hepatitis C patients has a proviral and anti-inflammatory effect. *Hepatology* **38**, 859-868 (2003).
45. J. Banchereau, R. M. Steinman, Dendritic cells and the control of immunity. *Nature* **392**, 245-252 (1998).
46. C. V. Harding, E. R. Unanue, Quantitation of antigen-presenting cell MHC class II/peptide complexes necessary for T-cell stimulation. *Nature* **346**, 574-576 (1990).
47. P. Kivisäkk *et al.*, Human cerebrospinal fluid central memory CD4+ T cells: evidence for trafficking through choroid plexus and meninges via P-selectin. *Proceedings of the National Academy of Sciences of the United States of America* **100**, 8389-8394 (2003).
48. R. C. Axtell, L. Steinman, Gaining entry to an uninflamed brain. *Nat Immunol* **10**, 453-455 (2009).
49. H. Iwai *et al.*, Tissue-resident M2 macrophages directly contact primary sensory neurons in the sensory ganglia after nerve injury. *J Neuroinflammation* **18**, 227 (2021).
50. J. Delon, N. Bercovici, R. Liblau, A. Trautmann, Imaging antigen recognition by naive CD4+ T cells: compulsory cytoskeletal alterations for the triggering of an intracellular calcium response. *Eur J Immunol* **28**, 716-729 (1998).
51. E. Donnadieu, G. Bismuth, A. Trautmann, Antigen recognition by helper T cells elicits a sequence of distinct changes of their shape and intracellular calcium. *Curr Biol* **4**, 584-595 (1994).
52. W. Lin *et al.*, Morphological change of CD4(+) T cell during contact with DC modulates T-cell activation by accumulation of F-actin in the immunology synapse. *BMC Immunol* **16**, 49 (2015).

53. S. Afroz *et al.*, CGRP Induces Differential Regulation of Cytokines from Satellite Glial Cells in Trigeminal Ganglia and Orofacial Nociception. *Int J Mol Sci* **20**, (2019).
54. O. Avraham *et al*., Satellite glial cells promote regenerative growth in sensory neurons. *Nat Commun* **11**, 4891 (2020).
55. P. Pierre *et al.*, Developmental regulation of MHC class II transport in mouse dendritic cells. *Nature* **388**, 787-792 (1997).
56. A. Chow, D. Toomre, W. Garrett, I. Mellman, Dendritic cell maturation triggers retrograde MHC class II transport from lysosomes to the plasma membrane. *Nature* **418**, 988-994 (2002).
57. M. M. Jurewicz, L. J. Stern, Class II MHC antigen processing in immune tolerance and inflammation. *Immunogenetics* **71**, 171-187 (2019).
58. D. Lankar *et al.*, Dynamics of major histocompatibility complex class II compartments during B cell receptor-mediated cell activation. *J Exp Med* **195**, 461-472 (2002).
59. K. Inaba *et al.*, The formation of immunogenic major histocompatibility complex class II-peptide ligands in lysosomal compartments of dendritic cells is regulated by inflammatory stimuli. *J Exp Med* **191**, 927-936 (2000).
60. T. T. Wang *et al.*, Activation of Different Heterodimers of TLR2 Distinctly Mediates Pain and Itch. *Neuroscience* **429**, 245-255 (2020).
61. J. S. Cameron *et al.*, Toll-like receptor 3 is a potent negative regulator of axonal growth in mammals. *J Neurosci* **27**, 13033-13041 (2007).
62. I. Barajon *et al.*, Toll-like receptors 3, 4, and 7 are expressed in the enteric nervous system and dorsal root ganglia. *J Histochem Cytochem* **57**, 1013-1023 (2009).
63. Z. Z. Xu *et al.*, Inhibition of mechanical allodynia in neuropathic pain by TLR5-mediated A-fiber blockade. *Nat Med* **21**, 1326-1331 (2015).
64. Z. J. Zhang *et al.*, TLR8 and its endogenous ligand miR-21 contribute to neuropathic pain in murine DRG. *J Exp Med* **215**, 3019-3037 (2018).
65. T. A. Szabo-Pardi, L. R. Barron, M. E. Lenert, M. D. Burton, Sensory Neuron TLR4 mediates the development of nerve-injury induced mechanical hypersensitivity in female mice. *Brain Behav Immun* **97**, 42-60 (2021).
66. S. A. Malin, B. M. Davis, D. C. Molliver, Production of dissociated sensory neuron cultures and considerations for their use in studying neuronal function and plasticity. *Nature Protocols* **2**, 152-160 (2007).
67. A. François *et al.*, The Low-Threshold Calcium Channel Cav3.2 Determines Low-Threshold Mechanoreceptor Function. *Cell Rep* **10**, 370-382 (2015).
68. C. C. Clement *et al.*, The Dendritic Cell Major Histocompatibility Complex II (MHC II) Peptidome Derives from a Variety of Processing Pathways and Includes Peptides with a Broad Spectrum of HLA-DM Sensitivity. *J Biol Chem* **291**, 5576-5595 (2016).
69. G. P. Mommen *et al*., Sampling From the Proteome to the Human Leukocyte Antigen-DR (HLA-DR) Ligandome Proceeds Via High Specificity. *Mol Cell Proteomics* **15**, 1412-1423 (2016).
70. C. Münz, Autophagy Beyond Intracellular MHC Class II Antigen Presentation. *Trends in immunology* **37**, 755-763 (2016).
71. A. K. H. Stavoe, E. L. F. Holzbaur, Autophagy in Neurons. *Annu Rev Cell Dev Biol* **35**, 477-500 (2019).
72. M. Draheim *et al.*, Profiling MHC II immunopeptidome of blood-stage malaria reveals that cDC1 control the functionality of parasite-specific CD4 T cells. *EMBO Mol Med* **9**, 1605-1621 (2017).
73. T. Fugmann, A. Sofron, D. Ritz, F. Bootz, D. Neri, The MHC Class II Immunopeptidome of Lymph Nodes in Health and in Chemically Induced Colitis. *J Immunol* **198**, 1357-1364 (2017).
74. I. Strug *et al.*, Vaccinia peptides eluted from HLA-DR1 isolated from virus-infected cells are recognized by CD4+ T cells from a vaccinated donor. *J Proteome Res* **7**, 2703-2711 (2008).
75. S. Gadgil *et al.*, A systematic summary and comparison of animal models for chemotherapy induced (peripheral) neuropathy (CIPN). *PLoS One* **14**, e0221787 (2019).
76. J. Schindelin *et al.*, Fiji: an open-source platform for biological-image analysis. *Nat Methods* **9**, 676-682 (2012).

Acknowledgments: We would like to thank the UNE COBRE Behavior Core, especially Dr. Tamara King and Denise Giuvelis, for running TPP and assisting in experimental design, analysis, and interpretation.

Funding:

National Institutes of Health grant R01CA267554 (DG)

National Institutes of Health grant P20GM103643 (IM, DG)

University of New England, Office of Sponsored Programs mini grant 17076 (DG)

Author contributions:

Conceptualization: DJG

Methodology: DJG, EEW, NEM

Software: EEW

Investigation: EEW, DJG, NEM

Validation: NEM, RCC

Visualization: DJG, EEW

Funding acquisition: DJG

Project administration: DJG

Supervision: DJG

Writing – original draft: EEW, DJG

Writing – review & editing: EEW, DJG, RCC

Competing interests: The authors declare no competing interests.

Data and materials availability: All data are available in the main text or the supplementary materials.

A. Day 14 PTX

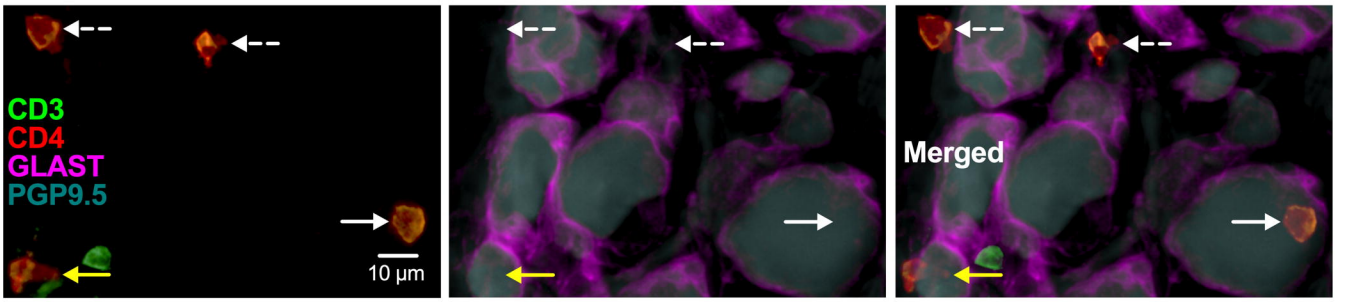

B. Day 14 PTX

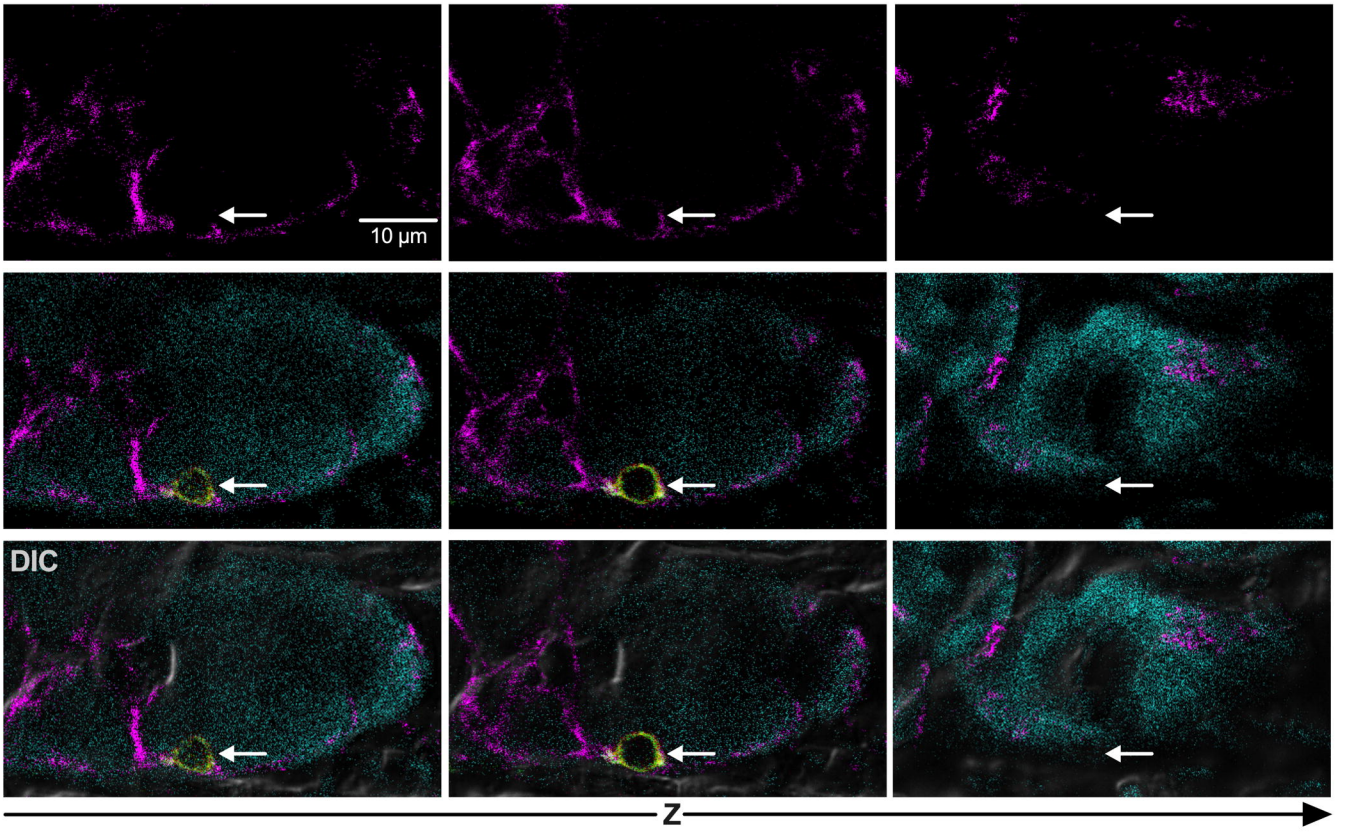

C. Naive

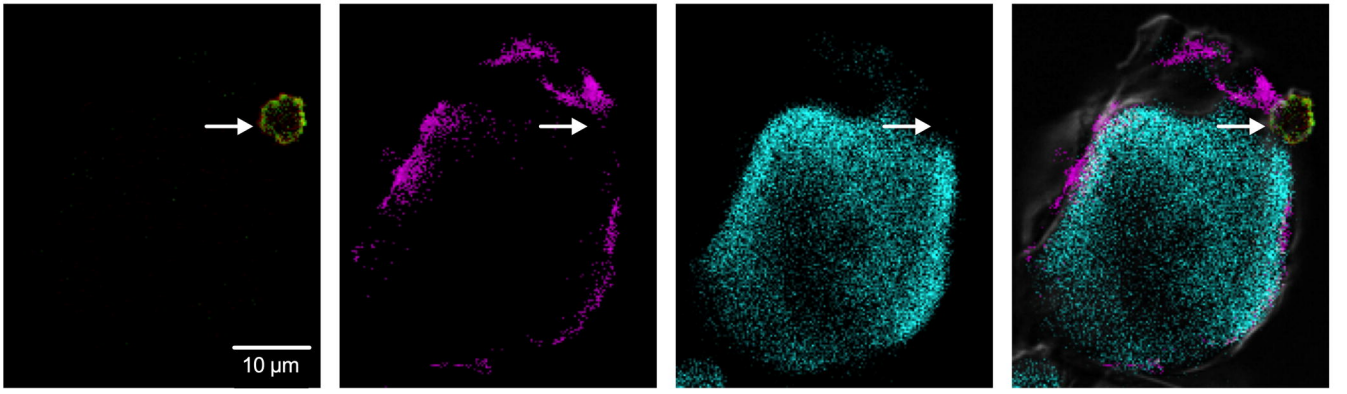

A.

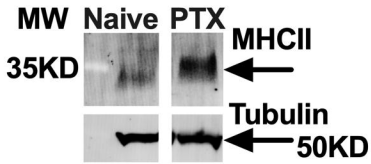
MW
Naive
PTX
35KD
MHCII
Tubulin
50KD

B.

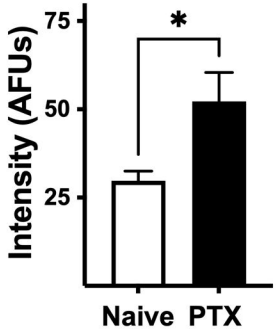
Intensity (AFUs)
75
50
25
*
Naive
PTX

C.

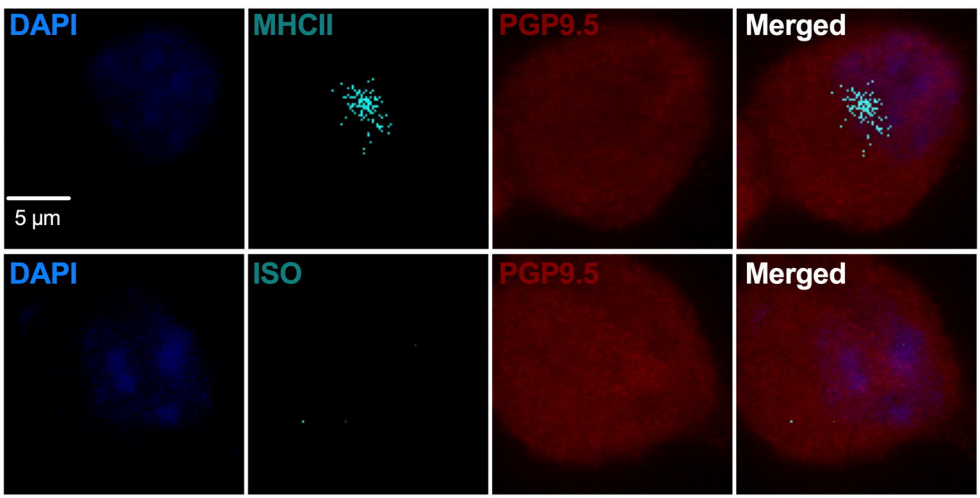
DAPI
MHCII
PGP9.5
Merged
5 µm
DAPI
ISO
PGP9.5
Merged

D.

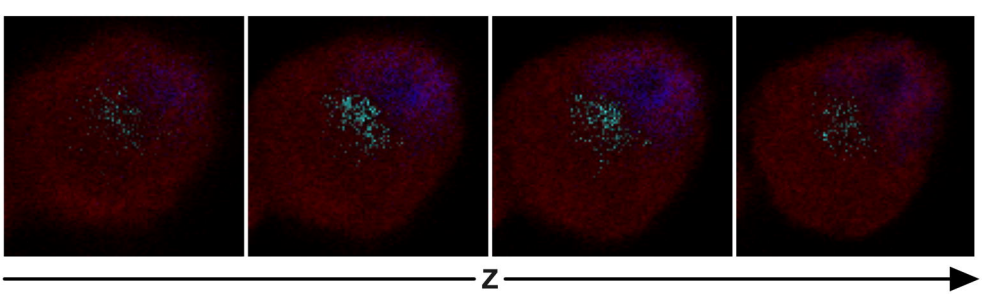
Z

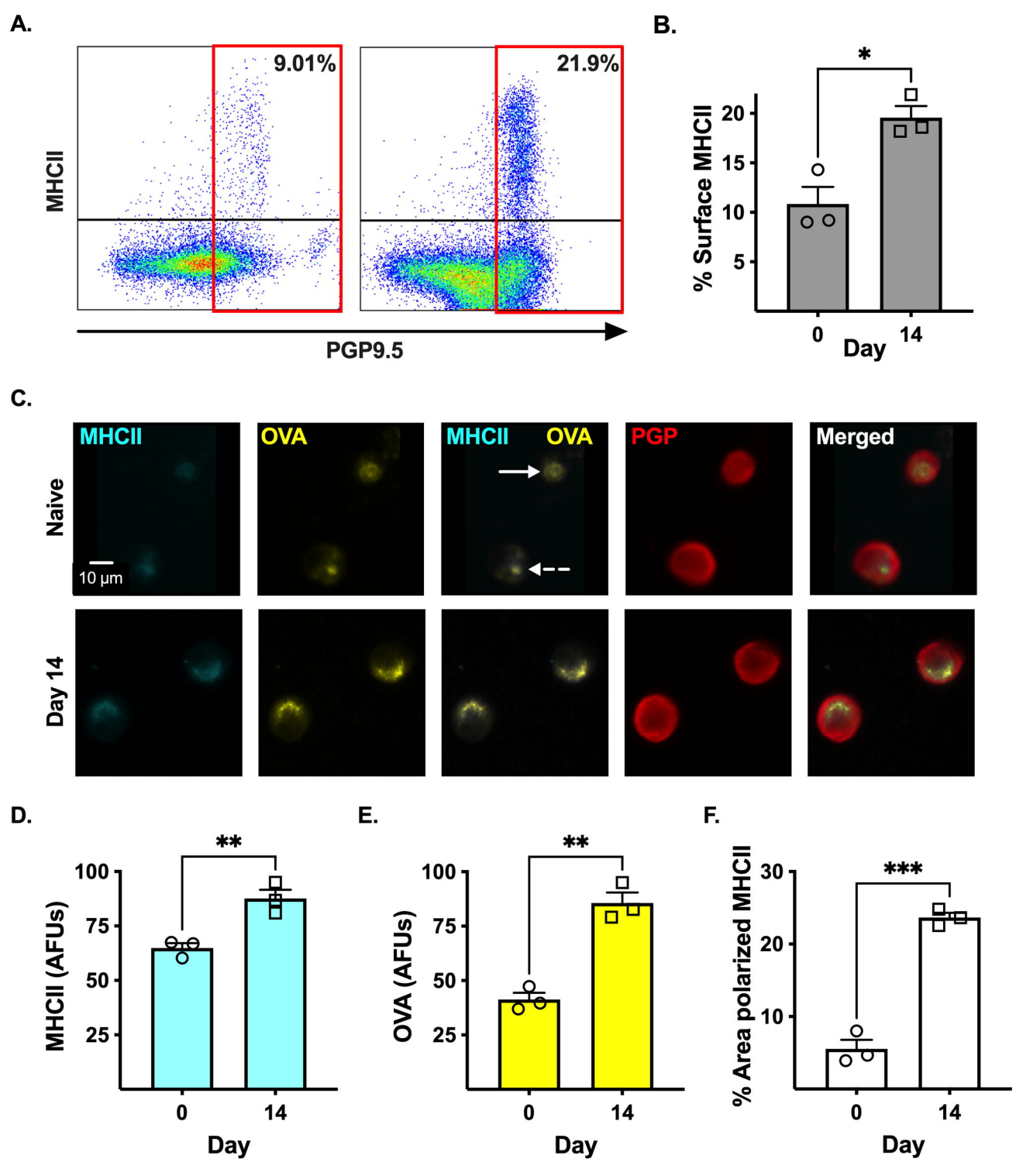
A.
9.01%
21.9%
MHCII
PGP9.5
B.
*
% Surface MHCII
20
15
10
5
0
14
Day
C.
MHCII
OVA
MHCII
OVA
PGP
Merged
Naive
10 µm
Day 14
D.
**
MHCII (AFUs)
100
75
50
25
0
14
Day
E.
**
OVA (AFUs)
100
75
50
25
0
14
Day
F.
***
% Area polarized MHCII
30
20
10
0
14
Day

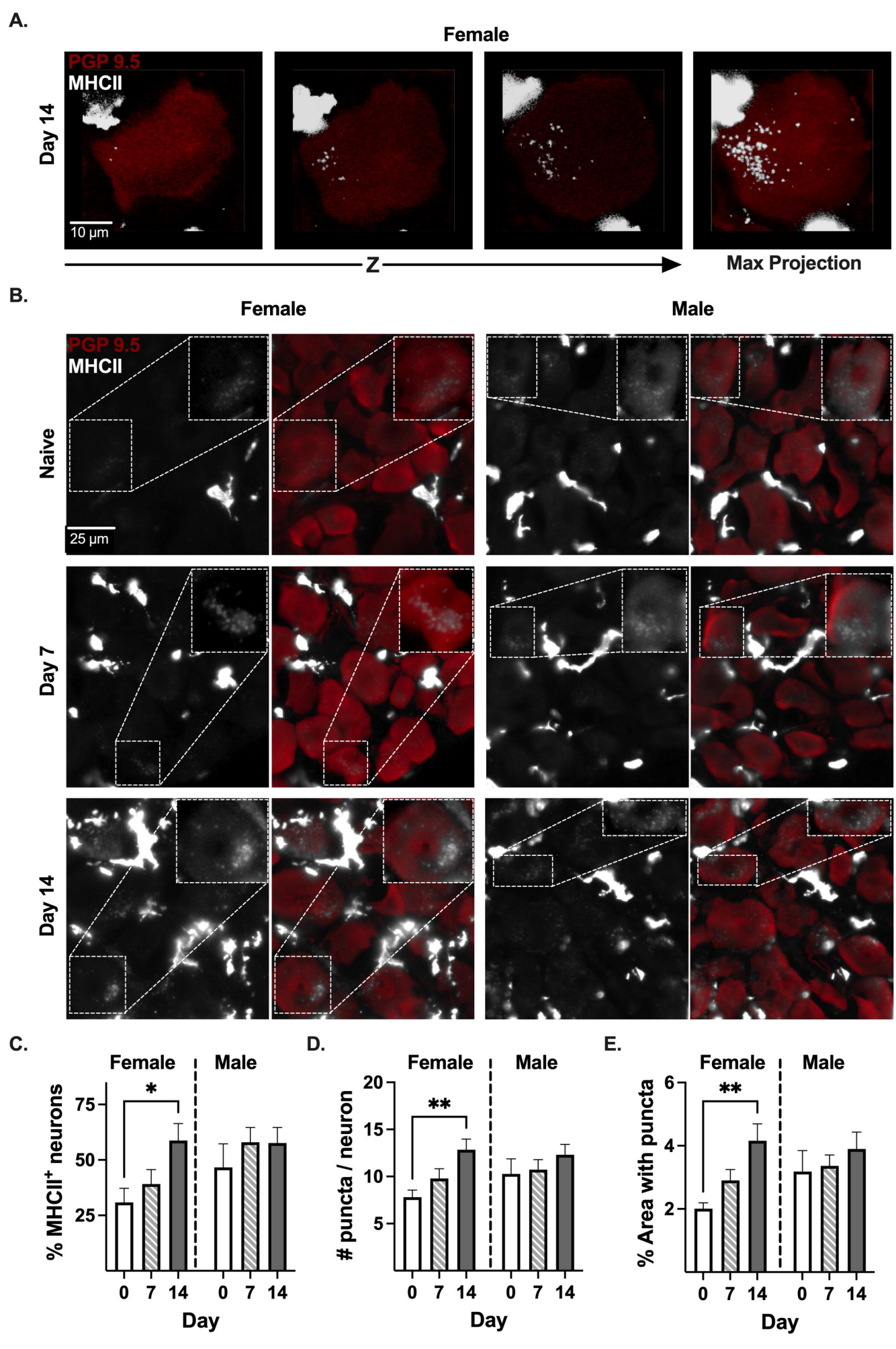
A.
Female
PGP 9.5
MHCII
Day 14
10 µm
Z
Max Projection
B.
Female
Male
PGP 9.5
MHCII
Naive
25 µm
Day 7
Day 14
C.
Female
Male
% MHCII+ neurons
75
50
25
*
0 7 14 0 7 14
Day
D.
Female
Male
puncta / neuron
20
15
10
5
**
0 7 14 0 7 14
Day
E.
Female
Male
% Area with puncta
6
4
2
**
0 7 14 0 7 14
Day

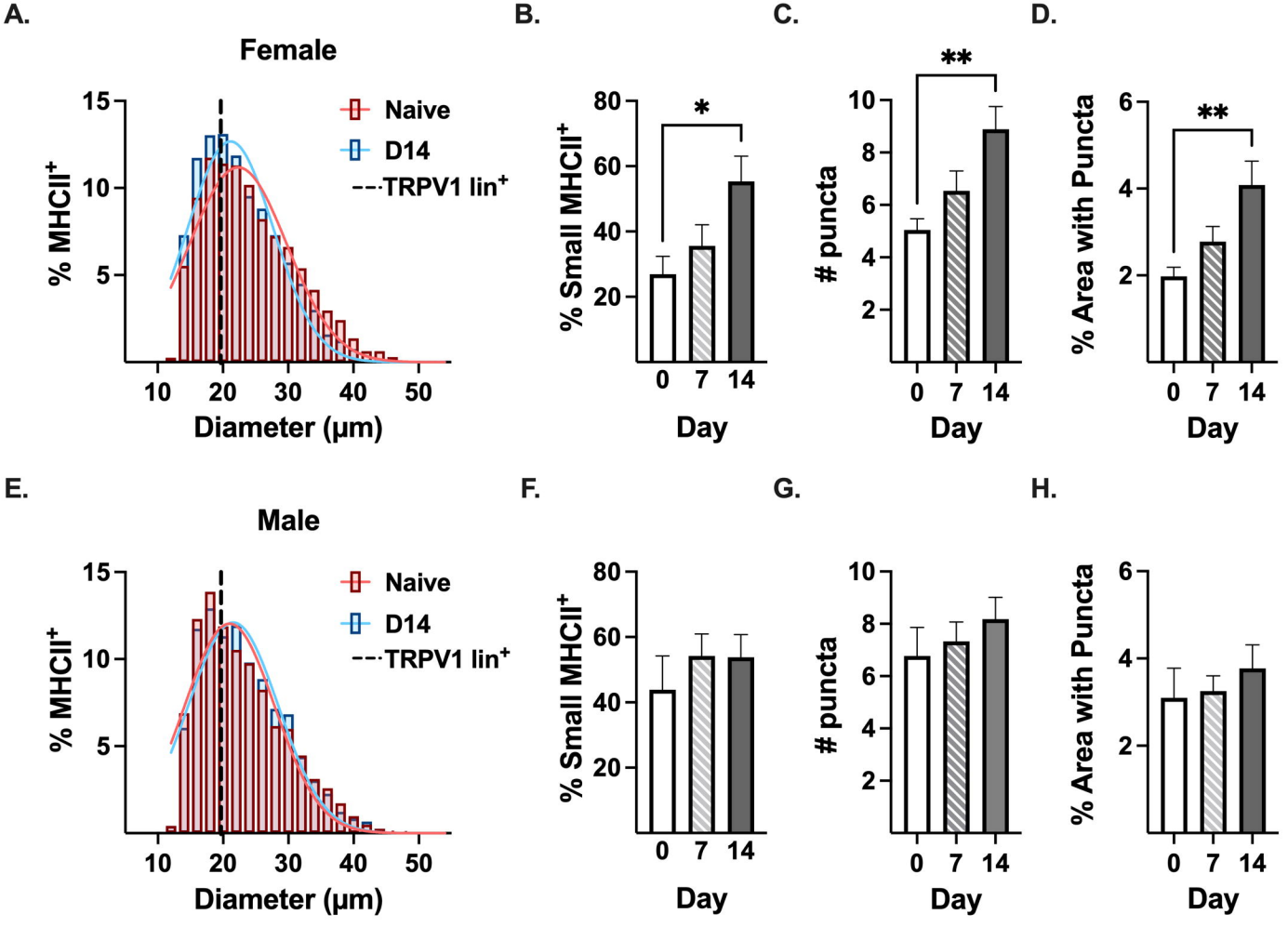
A.
Female
Naive
D14
TRPV1 lin+
% MHCII+
Diameter (μm)
B.
% Small MHCII+
Day
C.
puncta
Day
D.
% Area with Puncta
Day
E.
Male
Naive
D14
TRPV1 lin+
% MHCII+
Diameter (μm)
F.
% Small MHCII+
Day
G.
puncta
Day
H.
% Area with Puncta
Day

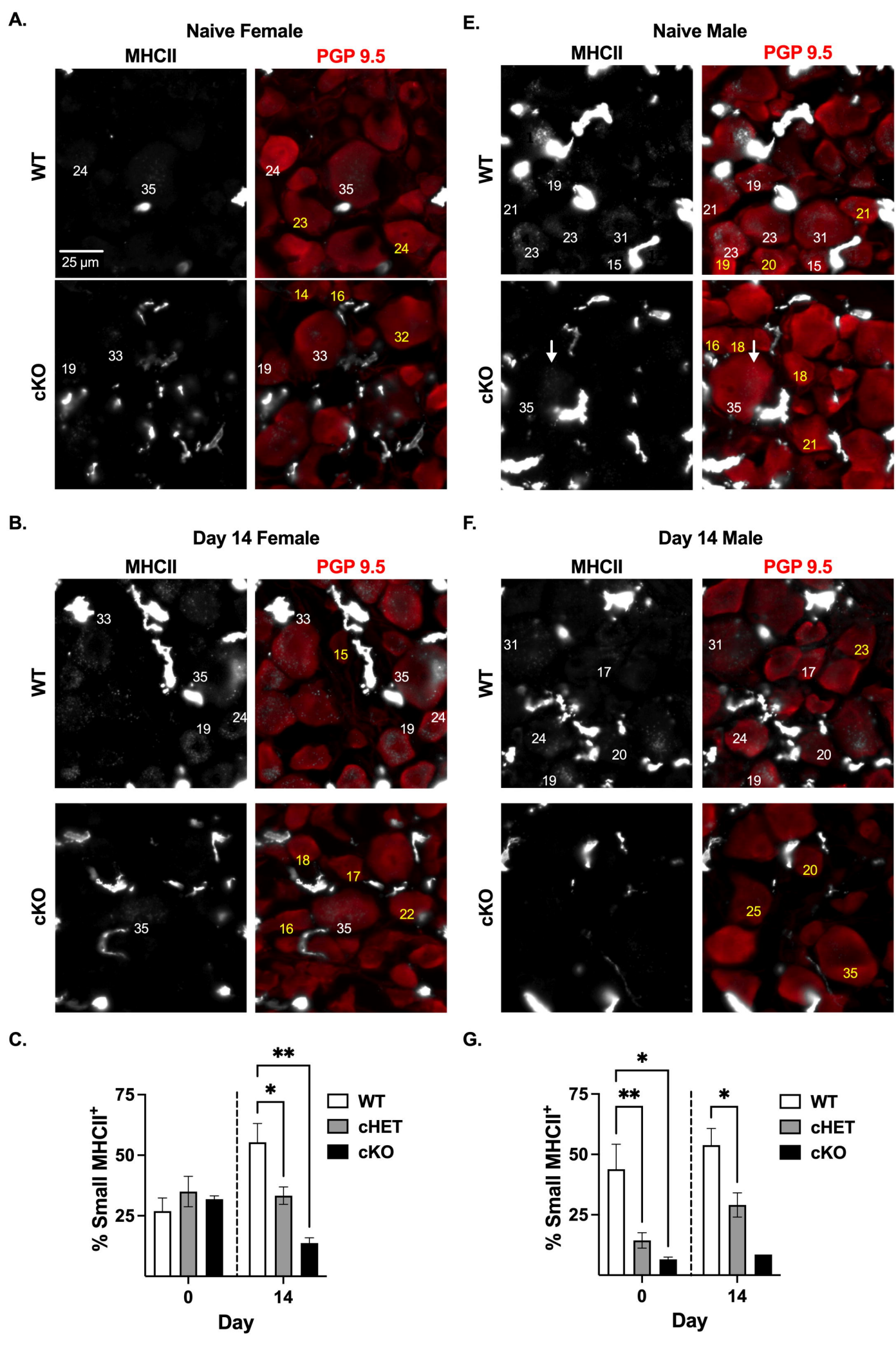
A.
Naive Female
MHCII
PGP 9.5
WT
cKO
25 µm
B.
Day 14 Female
C.
% Small MHCII+
Day
WT
cHET
cKO
E.
Naive Male
F.
Day 14 Male
G.

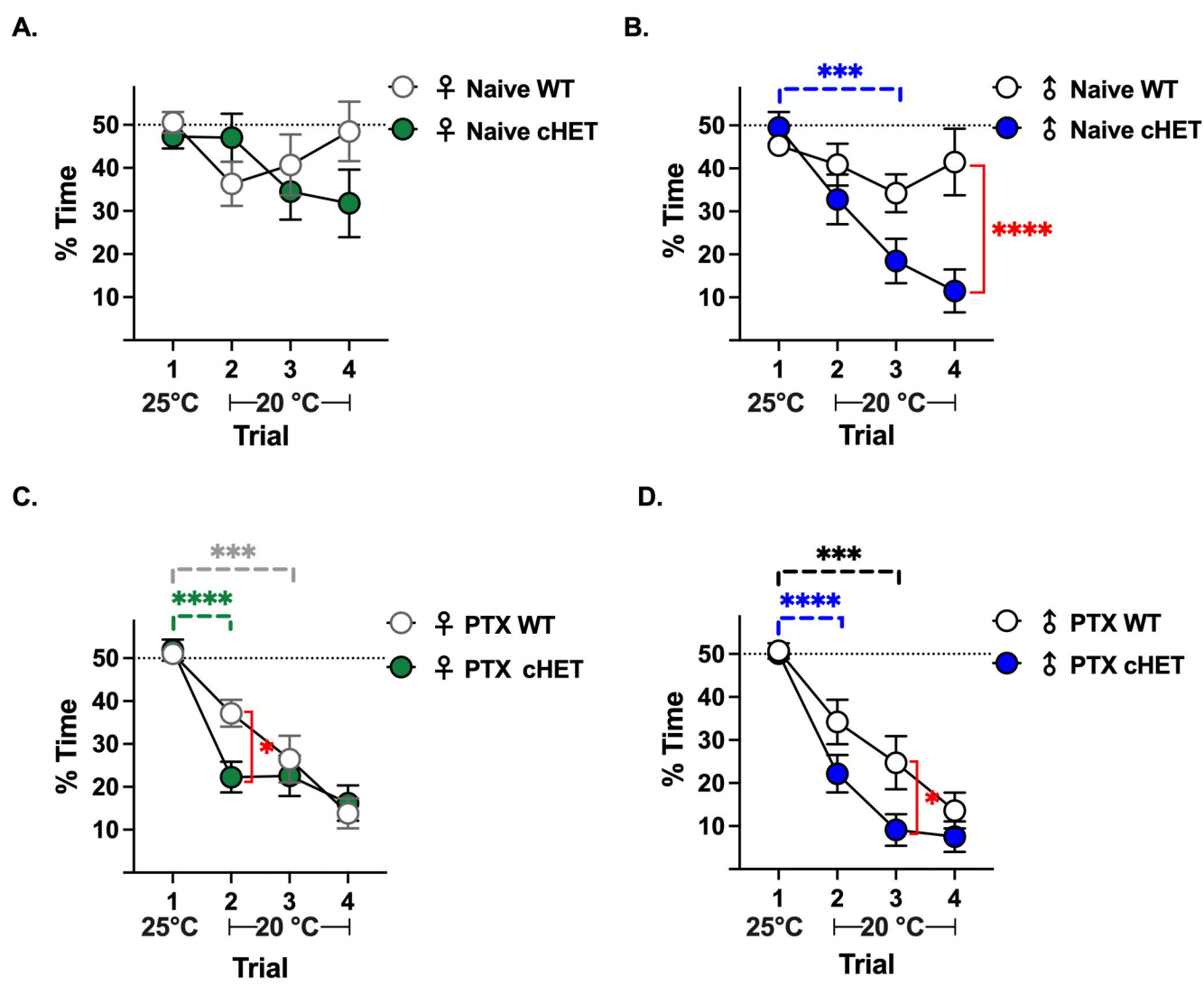
A.
Naive WT
Naive cHET
% Time
50
40
30
20
10
1
2
3
4
25°C
20 °C
Trial
B.
***
****
Naive WT
Naive cHET
% Time
Trial
C.
***
****
*
PTX WT
PTX cHET
% Time
Trial
D.
***
****
*
PTX WT
PTX cHET
% Time
Trial

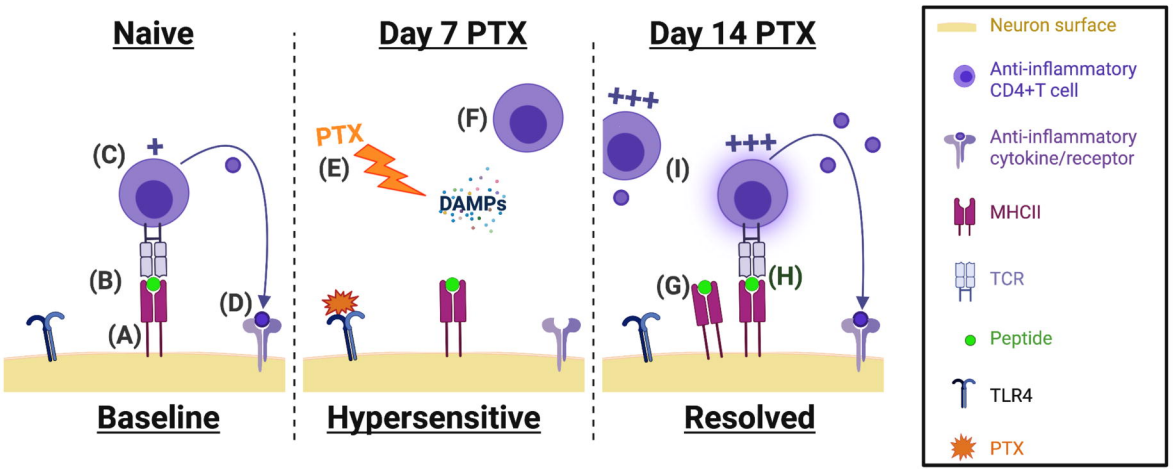
Naive
Day 7 PTX
Day 14 PTX
(C)
+
(B)
(A)
(D)
PTX
(E)
(F)
DAMPs
+++
(I)
+++
(G)
(H)
Baseline
Hypersensitive
Resolved
Neuron surface
Anti-inflammatory CD4+T cell
Anti-inflammatory cytokine/receptor
MHCII
TCR
Peptide
TLR4
PTX